







ARTICLE

CDKD-dependent activation of CDKA;1 controls microtubule dynamics and cytokinesis during meiosis

Kostika Sofroni¹, Hiroto Takatsuka², Chao Yang¹, Nico Dissmeyer³, Shinichiro Komaki², Yuki Hamamura¹, Lev Böttger¹, Masaaki Umeda², and Arp Schnittger¹

Precise control of cytoskeleton dynamics and its tight coordination with chromosomal events are key to cell division. This is exemplified by formation of the spindle and execution of cytokinesis after nuclear division. Here, we reveal that the central cell cycle regulator CYCLIN DEPENDENT KINASE A;1 (CDKA;1), the *Arabidopsis* homologue of Cdk1 and Cdk2, partially in conjunction with CYCLIN B3;1 (CYCB3;1), is a key regulator of the microtubule cytoskeleton in meiosis. For full CDKA;1 activity, the function of three redundantly acting CDK-activating kinases (CAKs), CDKD;1, CDKD;2, and CDKD;3, is necessary. Progressive loss of these genes in combination with a weak loss-of-function mutant in *CDKA;1* allowed a fine-grained dissection of the requirement of cell-cycle kinase activity for meiosis. Notably, a moderate reduction of *CDKA;1* activity converts the simultaneous cytokinesis in *Arabidopsis*, i.e., one cytokinesis separating all four meiotic products concurrently into two successive cytokineses with cell wall formation after the first and second meiotic division, as found in many monocotyledonous species.

Introduction

Meiosis is a specialized type of cell division in which two rounds of chromosome segregation events, meiosis I and meiosis II, follow a single round of DNA replication, resulting in a reduction of the DNA content by half. By this, meiosis maintains genome size in sexually reproducing organisms from one generation to the next, since the full DNA content of an organism is restored after the fusion of the female and male gametes. Moreover, meiosis is a driving force for genetic diversity. First, homologous chromosomes exchange DNA segments during early prophase I through crossing over, thus creating a novel composition of genetic alleles. Second, all homologous chromosome pairs are randomly separated at the end of meiosis I, thereby forming new, yet complete, chromosome sets in daughter cells.

Both processes, the reduction in ploidy and meiotic recombination, require an elaborate behavior of chromosomes. For instance, homologous chromosomes must recognize each other in early prophase I and undergo pairing, whereas they need to be separated and equally distributed to opposite cell poles later in meiosis I. A key component facilitating homology search and pairing of chromosomes by promoting nuclear rotations, and

separation of chromosomes by building the spindles, as well as many other aspects of meiosis, is the microtubule cytoskeleton (Ding et al., 1998; Yoshida et al., 2013; Tapley and Starr, 2013; Christophorou et al., 2015). Consistent with their many functions, microtubule assemblies undergo dramatic changes during meiosis, as revealed by live-cell imaging (Mogessie et al., 2018; Prusicki et al., 2019). However, much of our understanding of the regulation of microtubules during cell division comes from studies of mitosis, and despite of its importance, it is far from understood how microtubule dynamics are controlled in meiosis.

A paradigm for the role of microtubules in mitosis is the formation of the phragmoplast in plants. The phragmoplast is a microtubule-based structure that serves to establish the new cell wall (cell plate) between the separated nuclei during plant cell division (Jürgens, 2005; Müller and Jürgens, 2016; Smertenko et al., 2017). Notably, some plant species skip phragmoplast formation and hence lack cytokinesis after the first meiotic division (meiosis I). Instead, four cell walls are concurrently formed after the second meiotic division (De Storme and Geelen, 2013). This type of cytokinesis, called simultaneous cytokinesis,

¹University of Hamburg, Department of Developmental Biology, Hamburg, Germany; ²Nara Institute of Science and Technology, Graduate School of Science and Technology, Nara, Japan; ³Department of Plant Physiology, University of Osnabrück, Osnabrück, Germany.

Correspondence to Arp Schnittger: arp.schnittger@uni-hamburg.de; H. Takatsuka's current address is School of Biological Science and Technology, College of Science and Engineering, Kanazawa University, Kanazawa, Japan.

© 2020 Sofroni et al. This article is distributed under the terms of an Attribution–Noncommercial–Share Alike–No Mirror Sites license for the first six months after the publication date (see <http://www.rupress.org/terms/>). After six months it is available under a Creative Commons License (Attribution–Noncommercial–Share Alike 4.0 International license, as described at <https://creativecommons.org/licenses/by-nc-sa/4.0/>).

which is characteristic for male meiosis in many dicotyledonous species, e.g., in the model plant *Arabidopsis thaliana* (De Storme and Geelen, 2013). In contrast, maize, rice, and wheat male meiocytes, representative for the majority of monocotyledonous plants, undergo cytokinesis after each division, referred to as successive cytokinesis (Furness and Rudall, 1999; Jürgens, 2005; Shamina et al., 2007). How the different cytokinesis programs are brought about is, up to now, not understood.

The dynamics of microtubules are controlled by many factors, notably kinases. Next to Aurora kinases and MAPKs, in particular cyclin-dependent kinase (CDK)-cyclin complexes have been found to regulate the microtubule cytoskeleton in mitosis (Dumitru et al., 2017; DeLuca et al., 2018; Vavrdová et al., 2019). CDKA;1, the major cell cycle CDK in *Arabidopsis* and the homologue of the animal kinase Cdk1 and Cdk2 (Nowack et al., 2012), was found to localize to several microtubule arrays in mitotic cells, especially to the preprophase band (Colasanti et al., 1993; Weingartner et al., 2001). Conversely, application of CDK inhibitors resulted in the loss of spindle polarity, and the expression of a nondegradable cyclin B1 version disrupted phragmoplast organization and caused cytokinetic defects (Binarová et al., 1998; Weingartner et al., 2004).

Although the regulation of microtubules by CDKA;1 in meiosis has not been studied so far, recent data implicated the meiotic A-type cyclin TARDY ASYNCHRONOUS MEIOSIS (TAM) in coordination of the microtubule cytoskeleton with nuclear processes in *Arabidopsis*. In *tam* mutants, ectopic anti-parallel microtubule bundles are formed that resemble the microtubule organization in the spindle and the phragmoplast. Notably, these structures appear before nuclear envelope breakdown (NEB) and are, after NEB, rapidly incorporated into the first meiotic spindle (Prusicki et al., 2019).

TAM has been found to build an active complex with CDKA;1 (Harashima and Schnittger, 2012; Cromer et al., 2012). Mutants with lowered CDKA;1 activity levels have reduced fertility and suffer from multiple defects in meiosis, including an altered meiotic recombination pattern (Dissmeyer et al., 2007, 2009; Wijnker et al., 2019). Consistent with its many functions, CDKA;1 is present throughout female and male meiosis (Bulankova et al., 2010; Zhao et al., 2012; Yang et al., 2020).

The dissection of the role of CDK-cyclin complexes in plants is complex, since besides TAM, there are >30 cyclins present in the *Arabidopsis* genome (Wang et al., 2004a). Among them, seven A- and B-type cyclins have been found to be expressed in male meiocytes, examples being SOLO DANCERS and CYCB3;1 (Bulankova et al., 2013), in addition to TAM. Whereas SOLO DANCERS has been found to play an important role in meiotic recombination (Azumi et al., 2002; Girard et al., 2015) not much is known about CYCB3;1, and single mutants of CYCB3;1 did not exhibit any obvious growth defect. However, ectopic and premature cell wall formation in meiocytes were found in the double mutants of the SOLO DANCERS gene (*sds*) and *cycb3;1* (Bulankova et al., 2013).

Besides the interaction with cyclin cofactors, CDKs are regulated by the binding of inhibitors and by phosphorylation (Morgan, 1997). Phospho-control of CDKs works at two levels in animals and yeast, i.e., by an inhibitory phosphorylation in the

P-loop and activatory phosphorylations in the T-loop (Morgan, 1997). However, there seem to be variations to this general scheme since, at least in *Arabidopsis*, CDKA;1 appears to be regulated only by T-loop phosphorylation and not by P-loop phosphorylation (Harashima et al., 2007; Dissmeyer et al., 2007, 2009; Bulankova et al., 2010).

T-loop phosphorylation of CDKA;1 is catalyzed by another class of CDKs, i.e., CDK-activating kinases (CAKs), e.g., the monomeric kinase CAK1 in budding yeast and Cdk7-cyclin H complexes in vertebrates (Kaldis, 1999). CAK activity is represented by the D-type CDKs in *Arabidopsis* that build a small gene family with three members, CDKD;1, CDKD;2, and CDKD;3, all of which form active complexes with the *Arabidopsis* cyclin H homologue (Shimotohno et al., 2003; Umeda et al., 2005). Single mutants in CDKDs do not show any obvious alterations from WT. However, double mutants *cdkd;1 cdkd;2* and *cdkd;2 cdkd;3* are reduced in growth and fertility, and the double mutant *cdkd;1 cdkd;3* is gametophytic lethal (Takatsuka et al., 2015; Hajheidari et al., 2012). Consequently, the triple mutant *cdkd;1 cdkd;2 cdkd;3* could also not be recovered. However, *cdkd;1 cdkd;2* could be combined with a weak loss-of-function allele of CDKD;3, named *cdkd3-2*, resulting in miniature plants that also showed defects in gametophyte development (Hajheidari et al., 2012).

Here, we have analyzed the function of CDKDs in meiosis. Removing CDKDs in a stepwise fashion allowed us to dissect their role in a very fine-grained manner. In particular, we found that microtubule organization is controlled by CDKA;1 in a CDKD activation-dependent mode. Strikingly, we observed that a slight reduction of CDKA;1 activity converted the simultaneous meiosis of *Arabidopsis* into a successive meiosis, indicating that small differences in CDKA;1 activity are fully sufficient to drastically alter meiotic progression.

Results

CDKDs are expressed during the entire meiosis and colocalize with CDKA;1 in the nucleus

To understand the role of CDKDs in meiosis, we first analyzed their localization pattern in male meiocytes. For this purpose, we generated genomic reporters in which the coding sequence of mVenus as a fluorescent marker was added directly before the stop codon of the three CDKD genes. Because single mutants in each of the CDKD genes do not lead to a mutant phenotype, we transformed these genomic constructs into the two double mutants *cdkd;1/- cdkd;3/+* and *cdkd;2/- cdkd;3/-*, which show reduced growth and have fertility defects (Hajheidari et al., 2012). Expression of these reporter lines completely rescued the *cdkd;1/- cdkd;3/+* and *cdkd;2/- cdkd;3/-* double mutant phenotypes, and we conclude that these reporters are fully functional (Fig. S1, A–E).

Because CDKD;2 was previously found to have high kinase activity against Cdk2, and because CDKA;1 and Cdk2 are homologous kinases (Shimotohno et al., 2006; Dissmeyer et al., 2007), we generated a genomic CDKA;1 reporter fused to mTurquoise2 (*PRO_{CDKA;1}CDKA;1:mTurquoise2*) to allow the concomitant analysis of CDKDs and CDKA;1. We judged the *PRO_{CDKA;1}CDKA;1:mTurquoise2* to be fully functional, since it

complemented the severe somatic growth reduction of *cdka1*–null mutants (Nowack et al., 2012) and restored the meiotic defects previously observed in weak loss-of-function *cdka1*–mutants (Dissmeyer et al., 2007; Wijnker et al., 2019; Yang et al., 2020; Fig. S1, F and G).

All three CDKDs localized to the nuclei of meiocytes (Fig. S2). As a representative example and for reasons presented below, we focused our analysis on CDKD;3. Fig. S2, A–F, shows the accumulation pattern of CDKD;3 and CDKA;1. During pre-meiosis, both CDKD;3 and CDKA;1 abundance levels were low (Fig. S2 A). In prophase I, accumulation of CDKD;3 increased, and it colocalized with the nuclear portion of CDKA;1 (Fig. S2, B–D). As revealed by colocalized pixel maps and scatter plot analyses, the level of colocalization is stage dependent: high at early and middle prophase I ($R_{\text{coloc}} = 0.915$ and 0.893 , respectively) and low at late prophase I ($R_{\text{coloc}} = 0.726$). This dynamics is at least in part due to a simultaneous increase of the cytoplasmic and a decrease of the nuclear portion of CDKA;1 as revealed by a recent ratiometric quantification of CDKA;1 abundance during meiosis (Yang et al., 2020). Later, CDKD;3 accumulated together with CDKA;1 in the newly formed nuclei after meiosis I (in interkinesis) and after meiosis II (in tetrads; Fig. S2, E and F). A very similar accumulation pattern was found for CDKD;1 and CDKD;2 (Fig. S2, G and H). Thus, CDKDs are present throughout meiosis, and the high level of colocalization is consistent with an *in vivo* interaction between CDKA;1 and all CDKDs in the nuclei of meiocytes, especially during prophase I.

Double mutants in CDKD genes have severe meiotic defects

The accumulation patterns of CDKDs suggested that all three proteins function in meiosis. To assess their role, we analyzed chromosome spreads of male meiocytes of single *cdkd* mutants in comparison with WT (Figs. 1 and S3, A and B).

Because none of the single *cdkd* mutants showed any obvious alteration from WT, consistent with no obvious reduction in fertility and growth of *cdkd* single mutants, we next studied double mutants. Neither *cdkd1*–*cdkd2*– nor *cdkd2*–*cdkd3*– homozygous double mutants showed an apparent difference in meiosis compared to WT (Fig. S3, C and D).

As the double homozygous mutant of *cdkd1*– and *cdkd3*– is gametophytic lethal (Takatsuka et al., 2015), we analyzed the combination of these mutants by keeping one of them in a heterozygous state. The first defects of *cdkd1 cdkd3* combinations became notable in metaphase I, when in WT and single *cdkd* mutants, five fully condensed bivalents are visible and are physically kept together by chiasmata as a result of crossing over (Fig. 1 A, first and second row). In *cdkd1*–*cdkd3*+/+ and *cdkd1*+/+*cdkd3*– double mutants, we observed univalents, indicating a failure of crossover formation between homologous chromosomes in these plants (red arrows in Fig. 1 A and red circles in Fig. 1 B). Although two pools of equally distributed chromosomes are visible in interkinesis of WT plants, we found unbalanced pools having a 6:4 or a 8:2 chromosome segregation in the *cdkd1 cdkd3* double mutants (39% of meiocytes with unbalanced chromosome pools in *cdkd1*–*cdkd3*+/+; 43% in *cdkd1*+/+*cdkd3*–) that persisted in metaphase II (Fig. 1, C and D). Additionally, chromosomes were still connected in the form of DNA bridges

(white arrows) at late stages of the second meiotic division (telophase II) after sister chromatids were already separated (Fig. 1, A and E). Notably, a WT phenotype was restored in the double *cdkd1*–*cdkd3* mutants when the genomic *CDKD1:mVenus* reporter construct was present (Fig. S3 E), confirming the functionality of this construct and corroborating that the meiotic defects seen in plants of *cdkd1 cdkd3* double-mutant combinations were due to the absence/reduction of CDKD activity. Taken together, these data demonstrate that CDKD;1 and CDKD;3 have a largely redundant role in crossover formation and chromosome segregation, with CDKD;3 being more important than CDKD;1.

Combined reduction of CDKD and CDKA activity results in a strongly enhanced mutant phenotype

A likely target of CDKD action, which could be responsible for the observed meiotic defects in *cdkd* mutants, is the major cell-cycle kinase CDKA;1 in *Arabidopsis* (Shimotomino et al., 2006; Nowack et al., 2012). One possibility to test this is by substituting in CDKA;1 the residue that is usually phosphorylated by CDKDs, i.e., Thr 161, with an amino acid that mimics phosphorylation, i.e., with a negative charge such as Asp or Glu (Dissmeyer et al., 2007; Harashima et al., 2007), and expressing this variant in the *cdkd* double mutants (Dissmeyer and Schnittger, 2011). However, such substitutions were previously generated and did not fully mimic T-loop phosphorylation of CDKA;1, resulting in CDKA;1 variants with reduced kinase activity (Dissmeyer et al., 2007; Harashima et al., 2007).

To assess the nature of a possible functional interaction between the two genes, we undertook a double-mutant analysis. To this end, we used a previously described *CDKA1* allele, called *CDKA1^{T14V;Y15F}* (hereafter VF), in which a *cdka1* null mutant carries the mutated *CDKA1* expression construct, resulting in a kinase variant with slightly reduced activity (Dissmeyer et al., 2009). Whereas *cdka1* mutants with very little kinase activity have severe meiotic defects, making it difficult to observe any possible enhancement of the mutant phenotype (Dissmeyer et al., 2007, 2009; Yang et al., 2020), VF *cdka1*– plants follow a meiotic course that is, at least qualitatively, similar to that in WT (compare the first row of Figs. 1 A and 2 B). Next, we combined VF *cdka1*– mutants with single mutants in *CDKD1* and *CDKD3*. The resulting double mutants displayed a progressive increase of meiotic defects depending on the degree of expression reduction (heterozygous versus homozygous) of the respective genes (Figs. 2 and S4).

When quantifying meiotic stages from metaphase I onward, as a rough estimate for the course of meiosis, we observed in WT that 10% of the meiocytes were in metaphase I, 20% in anaphase I/telophase I, 30% in interkinesis, 13% in metaphase II, and 27% in tetrad stage (Fig. 2 A). A similar distribution was found in VF *cdka1*– single mutants (Fig. 2 A). However, in the combination of VF *cdka1*– with heterozygous *cdkd3*+/+ mutants (called VF *cdka1*–*cdkd3*+/+), 55% of the 275 analyzed meiocytes were in interkinesis, and the number of cells undergoing the second meiotic division was strongly decreased (from 40% in WT to 16% in the double mutant; Fig. 2 A).

When *cdkd3* was a homozygous mutant in a VF *cdka1*– background (called VF *cdka1*–*cdkd3*–), meiocytes in the

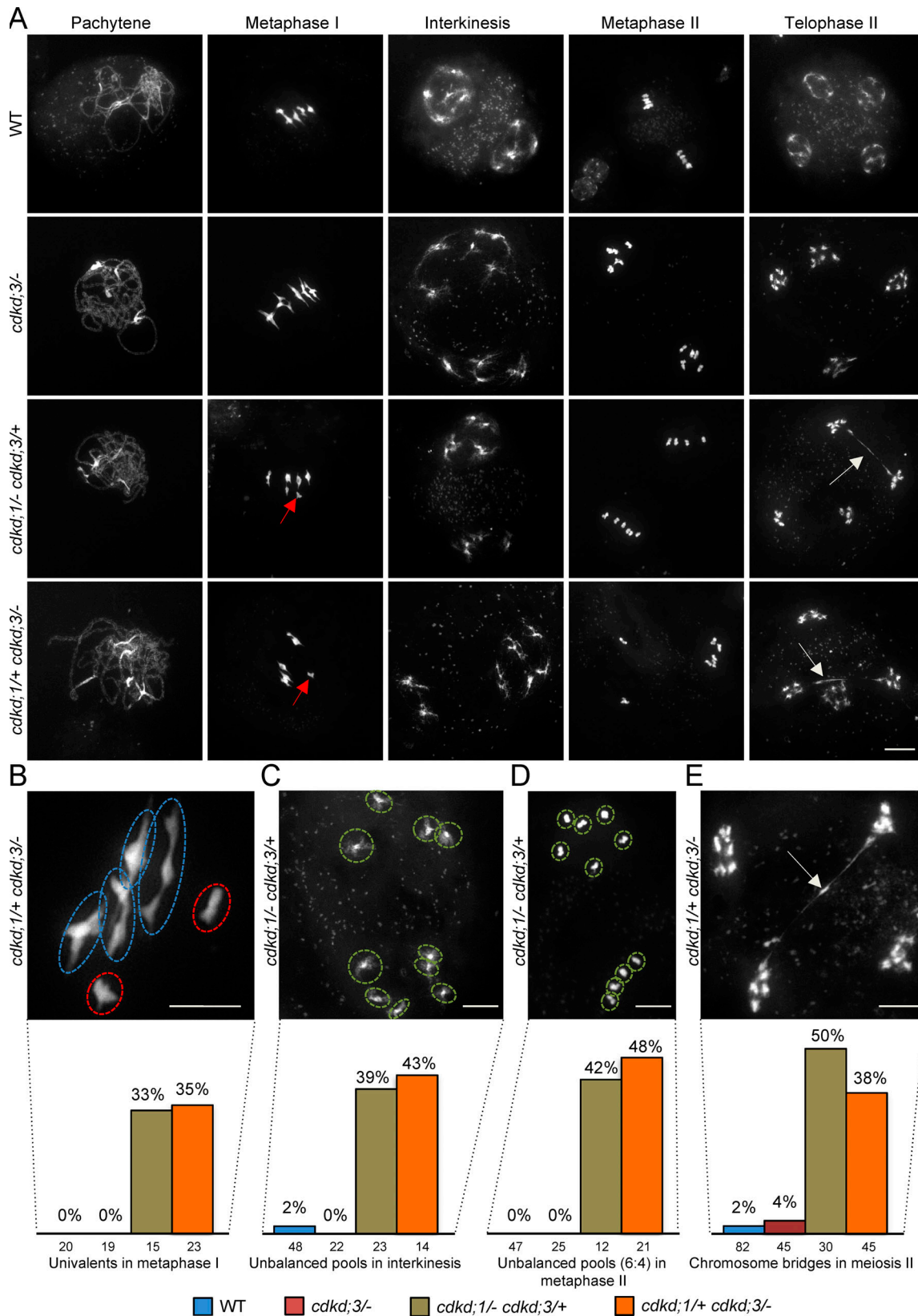


Figure 1. **Analysis of meiotic defects in *cdkd* mutants.** (A) Chromosome spread analysis of male meiocytes in WT versus single *cdkd;3* mutants and two different double *cdkd;1 cdkd;3* mutant combinations during pachytene, metaphase I, interkinesis, metaphase II, and telophase II. Red arrows indicate univalents in metaphase I, and white arrows designate chromosome bridges in telophase II. (B) Close-up of chromosomes with missing chiasmata in metaphase I of *cdkd;1/+ cdkd;3/-*. Red circles highlight univalents, and blue circles, bivalents. (C-E) Unbalanced chromosome pools in interkinesis (C) and metaphase II (D), and a chromosome bridge in telophase II (E) in *cdkd;1/+ cdkd;3/-* double mutants. In the last row, quantification of meiotic defects

observed in *cdkd;3/-* ($n = 66$), *cdkd;1/- cdkd;3/+* ($n = 50$), and *cdkd;1/+ cdkd;3/-* ($n = 58$) versus WT ($n = 115$). The numbers under every column indicate the meiocytes found per stage. Scale bar, 10 μm .

second meiotic division could not be found, and the number of meiocytes in interkinesis increased even further (Fig. 2 A). Concomitantly, we observed in these mutants a significant increase in seed abortion (Fig. S4, A and B) and a drastic decrease in pollen viability (Fig. S4 C). Moreover, we saw that the size of viable pollen grains became enlarged (Fig. S4 D). Typically, pollen size correlates very well with nuclear DNA content (De Storme et al., 2007), and the observed increase in size of the viable pollen from *VF cdkd;1/- cdkd;3* plants was similar to that observed in tetraploid WT plants (Fig. S4, D and E). Taken together, these results suggest that reduced CDKD activity results in diminished activation of CDKA;1, leading to incomplete meiotic progression and ploidy defects in the progeny (as detailed below).

To test whether reduced T-loop phosphorylation of CDKA;1 in *cdkd* mutants could especially affect the activity of the CDKA;1 VF variant, we generated a triple-mutated CDKA;1 version (called VFD in the following), in which we used the VF variant and substituted Thr161 with Asp, which we knew from previous experiments cannot fully mimic a phosphorylated Thr residue in the context of the T-loop of CDKA;1 (CDKA;1 D variant; Dissmeyer et al., 2007). Whereas *VF cdkd;1/-* plants show no obvious reduction in growth and fertility, *D cdkd;1/-* plants are stunted and completely sterile (Dissmeyer et al., 2007, 2009). *VFD cdkd;1/-* plants were even more compromised than *D cdkd;1/-* plants, resembling *cdka;1* null mutants, with the exception of a root being formed in *VFD* but not in *cdka;1* null mutants (Fig. 3, A and C; Nowack et al., 2012; Weimer et al., 2012). Kinase assays from *VFD cdkd;1/-* plants revealed that this CDKA;1 variant has very low kinase activity, consistent with the severe mutant phenotype of these plants (Fig. 3 D). Thus, although the structural effects of the VFD mutations in CDKA;1 are not fully clear, the observed high sensitivity of CDKA;1 VF variant toward the presumptive reduction of T-loop phosphorylation in *cdkd* mutants is consistent with the strong defects of *VFD cdkd;1/-* plants and further supports the idea that CDKA;1 is an in vivo target of CDKDs.

To get a more detailed understanding of the mutant phenotypes of *VF cdkd* plants, we next performed chromosome spreads. In *VF*, meiotic progression was similar to the above-described chromosome spreads of WT (compare the first rows of Figs. 1 A and 2 B). In *VF cdkd;1/- cdkd;3/+*, chromosomes are paired at pachytene, but the presence of univalents (red arrows in Fig. 2 B) in 28% of cases in metaphase I indicated a reduction of crossover formation (Fig. 2 C). In anaphase I, we observed chromosome bridges, indicating unresolved crossovers (Fig. 2, B and C). In addition, the organellar band, separating the two pools of chromosomes in interkinesis in WT, was not found in *VF cdkd;1/- cdkd;3/+* (Fig. 2 B). Furthermore, we observed micronuclei at interkinesis-like stages (Fig. 2 B, blue arrow, and Fig. 2 C). The second meiotic division was strongly affected, as seen by very irregular chromosome figures in metaphase II,

unbalanced segregation of chromosomes, and chromosome bridges in late meiosis (Fig. 2 B, second row, and Fig. 2 C).

In *VF cdkd;1/- cdkd;3/-* plants, in which CDKD levels were further reduced, univalents at metaphase I and chromosome fragments at anaphase I were observed (Fig. 2 B, third row, and Fig. 2 C). Premature cell wall formation (Fig. 2 B, orange arrows) and exit of meiosis after meiosis I were observed in 83% of the cells, presumably leading to meiotic products with a greater than haploid nuclear DNA content, consistent with the above pollen size measurements (Fig. 2 B, third row; Fig. 2 C; and Fig. S4 E).

Notably, the combined reduction/loss of CDKA;1 and CDKD;3 activity went much beyond a simple additive mutant phenotype. For instance, whereas *cdkd;3/-* mutants show no univalents in metaphase I and *VF cdkd;1/-* plants have univalents in only 2% of all metaphase cells, 28% of all meiocytes in metaphase I of the mutant combination *VF cdkd;1/- cdkd;3/+* have univalents (Fig. 2 C). This value increased even further in the *VF cdkd;1/- cdkd;3/-* double mutant, to 66% of all meiocytes. A similar dosage dependence and great enhancement much exceeding an additive effect were observed for all meiotic phenotypes quantified in *VF cdkd;1 cdkd;3* combinations, i.e., chromosome bridges in anaphase I, unbalanced pools of chromosomes/micronuclei in interkinesis, exit after meiosis I, irregular metaphase II, and irregular tetrads (Fig. 2 C).

Additionally, we analyzed the combinations *VF cdkd;1/- cdkd;1/+* and *VF cdkd;1/- cdkd;1/-* (Fig. S4, F and G). Whereas meiotic progression was not affected in *VF cdkd;1/- cdkd;1/+* (Fig. S4 G, first row), double homozygous mutants showed premature cell wall formation (orange arrows) at interkinesis in 75% of cases (Fig. S4 G, second row). Taken together, these data show that the combined reduction of CDKA;1 and CDKD activity strongly enhanced the mutant phenotypes seen in hypomorphic *VF cdkd;1* mutants, indicating that CDKDs, especially CDKD;3, act as CDKA;1 activating kinases in meiosis.

CDKD;3 and CDKA;1 regulate microtubule organization in prophase I

To obtain further insights into the course of meiosis in *cdkd* mutants and their combination with *VF cdkd;1/-*, we introgressed the KINGBIRD reporter line into *VF cdkd;1/-* and *VF cdkd;1/- cdkd;3*. The KINGBIRD line holds a combination of two fluorescent reporters, one for the microtubule cytoskeleton, i.e., *PRO_{RPS5A}:TagRFP:TUA5*, and the other for chromatin, by labeling the α kleisin subunit of the meiosis-specific cohesion complex, i.e., *PRO_{REC8}:REC8:GFP* (Prusicki et al., 2019).

We first focused on prophase I. In WT, the nucleus moves to one side of the meiocyte in the zygotene, and microtubules progressively accumulate around the nucleus starting from the side of the nucleus that faces the cytoplasm, giving rise to a half-moon-like appearance (Fig. 4 A, light blue arrow; Prusicki et al., 2019). In late prophase I, this process is completed, and distinct arrays of microtubules embrace the entire nucleus (Fig. 4 B).

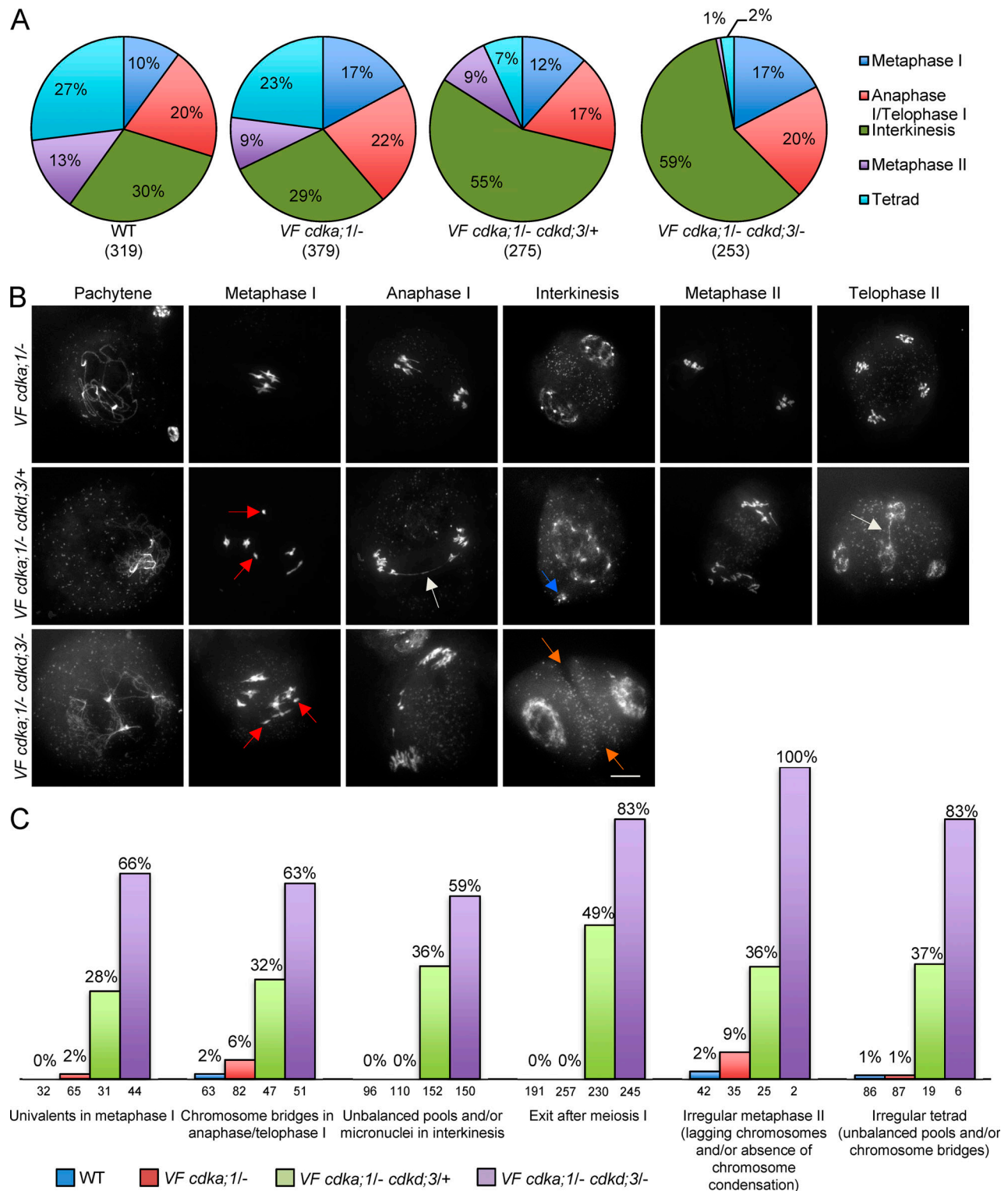


Figure 2. **Analysis of meiotic defects in *VF* and *VF cdk3* double mutant combinations.** (A) Repartition of meiotic stages within one single flower bud undergoing meiosis from metaphase I to telophase II/tetrad stage in WT ($n = 319$), *VF cdk1* ($n = 379$), *VF cdk1*; *1- cdk3*+ ($n = 275$), and *VF cdk1*; *1- cdk3*- ($n = 253$). (B) Chromosome spreads of male meiocytes in *VF cdk1* and *VF cdk1 cdk3* double mutants. Red arrows indicate univalents/fragments in metaphase I, white arrows pinpoint chromosome bridges in anaphase I and/or telophase II, blue arrows highlight micronuclei in interkinesis, and orange arrows point to premature cell wall formation in interkinesis. Scale bar, 10 μ m. (C) Quantification of meiotic defects observed in *VF cdk1*; *1- cdk3* double mutants versus WT given in percentage of meiocytes of one genotype that show the respective feature. The numbers under every column indicate the meiocytes found per stage.

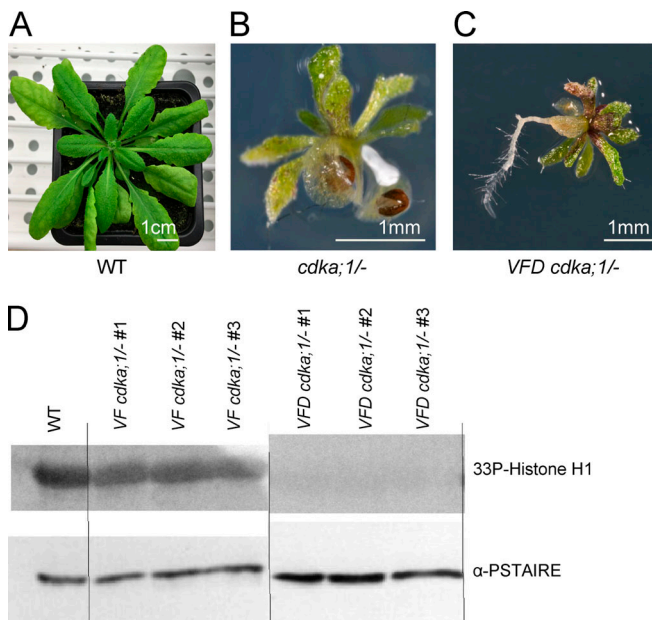


Figure 3. Characterization of the *VFD cdk;1* mutant. (A–C) Comparison between a WT *Arabidopsis* plant (A), the *cdk;1/-* null mutant (B), and the *cdk;1/- VFD* mutant (C). The *cdk;1/- VFD* mutants are reduced in growth to a similar extent as the homozygous *cdk;1* mutant but develop a root. (D) Upper row: CDK-kinase assays with plant material of WT, *VF cdk;1/-*, and *VFD cdk;1/-* using bovine histone H1 as a substrate. Lower row: CDKA;1 protein levels per kinase assay were visualized using an α-PSTAIRES antibody.

After NEB in diakinesis, the first spindle structures become visible (Fig. 4 C).

We found that the microtubule structures in *VF cdk;1/-* in combination with *cdkd;3* were affected in a dosage-dependent manner. Although the half-moon configuration of microtubules was less prominent in *VF cdk;1/- cdkd;3/+* than in WT (Fig. 4 D), it appeared to be completely lost in *VF cdk;1/- cdkd;3/-* (Fig. 4 G). Similarly, the microtubule structure that embraces the whole nucleus in later prophase I progressively diminished as CDKD;3 levels were further reduced in the context of *VF cdk;1/-* (Fig. 4, E and H), i.e., tubulin displayed a less bundled localization pattern in comparison with WT, as quantified by linescan intensity plots (Fig. 4, B', E', H', and J).

In addition, *VF cdk;1/- cdkd;3/-*, but not *VF cdk;1/- cdkd;3/+*, mutants showed ectopic antiparallel microtubule bundles at late prophase I, i.e., before NEB, resembling the microtubule organization in the phragmoplast and as also recently seen in *tam* mutants (Prusicki et al., 2019). These structures are described in more detail below. Thus, the organization of microtubules in prophase I strongly depends on the dosage of CDKA;1 and CDKDs.

The levels of CDKD;3 and CDKA;1 determine the pattern of cytokinesis

Next, we investigated microtubule localization after prophase I. In WT, microtubules reorganize after diakinesis to form the first meiotic spindle in metaphase I (Fig. 4 C). After interkinesis (Fig. 4 K), microtubules rearrange to form two perpendicularly

oriented spindles (Fig. 4, L and S), leading to the formation of a tetrahedral tetrad (Fig. 4, M and T). Strikingly different microtubule configurations were found in *VF cdk;1/-* mutants in combination with *cdkd;3*. In the *VF cdk;1/-* plants with reduced CDKD;3 activity (*VF cdk;1/- cdkd;3/+* and *VF cdk;1/- cdkd;3/-*), unattached fibers and irregular spindle structures were found (Fig. 4, F and I, yellow arrows). At later stages, consistent with our chromosome spread analysis (Fig. 2 B), premature exit after the first meiotic division led to the formation of dyads in *VF cdk;1/- cdkd;3/-*, as judged by the morphology and size of the cells (Fig. 4 Q).

Most interestingly, a different situation appeared in *VF cdk;1/- cdkd;3/+*, i.e., in plants with a moderate reduction of CDKD;3 activity. Here, microtubules bundled in interkinesis in the midzone (Fig. 4 N, red arrow) and progressively disappeared from outside to the inside of the meiocyte (Fig. 4 O). Subsequently, two rather parallel-oriented spindles were formed in 67% of cases (Fig. 4, P, U, and Y), giving rise to a planar tetrad (Fig. 4 V), while two rather perpendicularly positioned spindles, reflecting WT-like spindle constellation and leading to a tetrahedral orientation of the tetrad, appeared in only 22% of cases (Fig. 4, W–Y).

This microtubule pattern suggested that there could be a cell division after the first meiotic division, and hence, a transformation of simultaneous into successive cytokinesis in male meiosis of *VF cdk;1/- cdkd;3/+*. To test this hypothesis, we followed meiosis in WT and *VF cdk;1/- cdkd;3* mutants by live-cell imaging based on a recently developed protocol (Prusicki et al., 2019). To this end, we combined a tubulin marker (TagRFP: TUA5) with a plasma membrane marker (GFP:SYPI32). SYPI32 is a syntaxin (Qa-SNARE) known to mediate membrane fusion, needed, for example, for secretion and building the cell plate during cytokinesis of somatic cells (Park et al., 2018).

In WT, the reorganization of microtubules after diakinesis until metaphase II (as outlined above) is very fast and takes place in a largely concerted manner in all meiocytes within one another (Fig. 5 A and Video 1 A). At the end of telophase II, four spores are simultaneously formed after the invagination of the plasma membrane in an outside-in direction through simultaneous cytokinesis (Fig. 5 A, last column). The total duration of meiosis from diakinesis until telophase II in WT was determined to be ~240 min (Fig. 5, E and I).

In *VF cdk;1/-*, similar to WT, all meiocytes within one anther concertedly progressed through metaphase I, interkinesis, metaphase II, and telophase II, with no obvious alteration of microtubule organization patterns and no significant differences in the duration of the first meiotic division compared with WT, i.e., 73 min in WT versus 80 min in the mutant (Video 1 B and Fig. 5, F and I). However, meiocytes of *VF cdk;1/-* plants spent more time in interkinesis than WT plants (160 min versus 70 min), and metaphase II appeared to be slightly extended, with 70 min in WT versus 89 min in *VF cdk;1/-* (Fig. 5, F and I).

Remarkably, live-cell imaging of *VF cdk;1/- cdkd;3/+* plants revealed cell wall deposition not only after anaphase II but also already after anaphase I (Fig. 5 B from Video 2, red arrows). Therefore, meiocytes did not exit meiosis after a premature cytokinesis after meiosis I as seen in mutants with a strong reduction of CDKD activity, i.e., *VF cdk;1/- cdkd;3/-* (see below). Instead, microtubules were rapidly organized in a ring-like

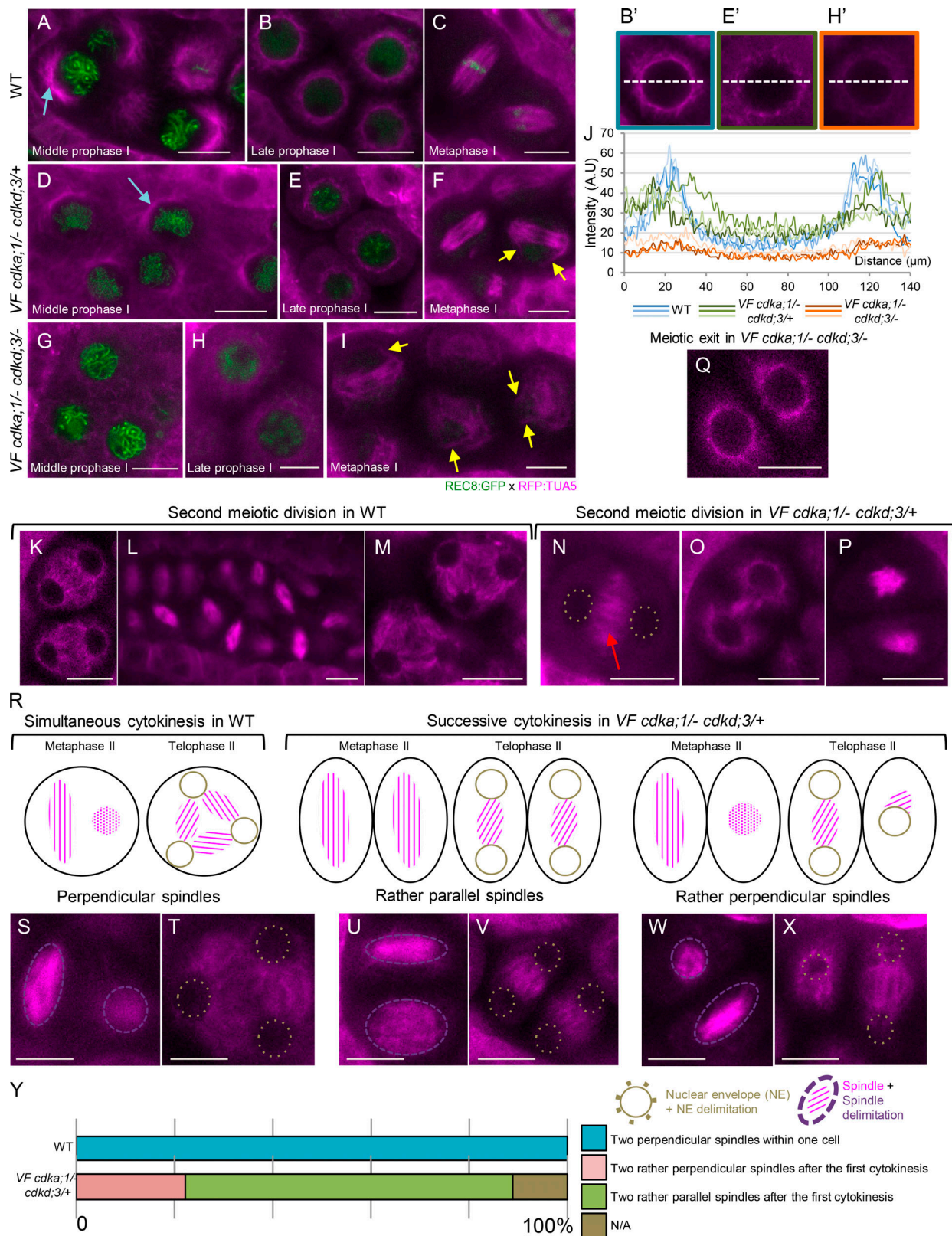


Figure 4. **Microtubule arrays in WT versus *VF cdk1-1 cdk3-3* mutants.** (A-I) Confocal laser scanning micrographs of meiotic cells expressing TagRFP:TUA5 (magenta) and REC8::GFP (green) from mid-prophase I to metaphase I in WT (A-C), *VF cdk1-1 cdk3-3/+* (D-F), and *VF cdk1-1 cdk3-3-/-* (G-I). Light-blue arrows indicate the half-moon configuration of microtubules present in WT that is lost in *VF cdk1-1 cdk3-3-/-*. The yellow arrows highlight irregular spindles in WT (B' and blue lines), *VF cdk1-1 cdk3-3/+* (E' and green lines), and *VF cdk1-1 cdk3-3-/-* (H' and orange lines) of a section going through the middle of the meiotic cell (white dotted line). (J, B', E', and H') Pixel intensity quantification from three meiotic cells at late prophase I in WT (B' and blue lines), *VF cdk1-1 cdk3-3/+* (E' and green lines), and *VF cdk1-1 cdk3-3-/-* (H' and orange lines) of a section going through the middle of the meiotic cell (white dotted line). (K-Q) After metaphase I, meiotic exit and dyad formation in *VF cdk1-1 cdk3-3-/-* (Q), second meiotic division in WT (K-M) and *VF cdk1-1 cdk3-3/+* (N-P). Red arrows indicate the

midzone microtubule array. **(R–X)** Schematic representation (R) of simultaneous cytokinesis in WT, which is characterized by two perpendicular spindles at metaphase II and a tetrahedral tetrad (S and T), versus successive cytokinesis in *VF cdka;1/- cdkd;3/+* mutant, in which the predominant spindle configuration is parallel, leading to a planar tetrad (U–X). **(Y)** Spindle orientation quantification for WT ($n = 40$) and *VF cdka;1/- cdkd;3/+* ($n = 36$). Scale bar, 10 μm .

structure around the nuclear envelope, similar to late prophase I. This microtubule configuration, unlike WT situation, persisted for a while and was then followed by the formation of a second spindle, in spatial configurations matching our above analysis (Fig. 5 B from Video 2; and Fig. 4, N–P and U–X). Consistent with an altered microtubule organization and precocious cell wall formation, we found that interkinesis is much longer in *VF cdka;1/- cdkd;3/+* plants, with 260 versus 70 min in WT (Fig. 5, G and I).

Thus, a concomitant reduction of CDKD and CDKA activity converts the simultaneous cytokinesis of *Arabidopsis* male meiocytes into successive cytokinesis, which is the predominant mode of division in male meiosis of monocotyledons (Furness and Rudall, 1999) and has been analyzed in detail, for example in maize (Nannas et al., 2016). This finding can also explain the occurrence of differently sized spores after meiosis in *VF cdka;1/- cdkd;3/+* plants (Fig. S4, D and E), i.e., one population of meiocytes that presumably terminates meiosis after the first division and a second that undergoes a second cell division.

In *VF cdka;1/- cdkd;3/-* plants, which have the lowest level of CDKD activity, we observed defective spindles and premature microtubule removal at the spindle midzone, followed by cell wall deposition (Fig. 5 C from Video 3, red arrows). Almost all meiocytes terminated meiosis after a long interkinesis, i.e., 250 versus 70 min in WT, and no second division was observed (Fig. 5, H and I).

Interestingly, in both mutant combinations, meiotic cell wall deposition still occurred in an outside-in direction (Fig. 5 D from Video 4, red asterisks). Thus, the observed successive cytokinesis and the premature cytokinesis followed by termination of meiosis after the first meiotic division display a similar mode of cleavage wall formation, as observed for the simultaneous cytokinesis in WT.

The pattern of MAP65 localization depends on CDKA;1 and CDKD activity

To further characterize the microtubule defects, we introgressed the microtubule binding protein MAP65-3 into *VF cdka;1/- cdkd;3/-* mutants. MAP65-3 has been shown to act as a bundling factor of antiparallel microtubules near their plus ends (Ho et al., 2012). In WT, MAP65-3 is clearly visible at late prophase I (Fig. 6 A) and localized together with tubulin in a full-moon-like conformation surrounding the nucleus shortly before NEB. In interkinesis, MAP65-3 accumulated in the midzone between the two nuclei (Fig. 6 B), and at the beginning of the second meiotic division, it was removed, following the pattern of microtubule removal, from the cell center to the side of the cell (Video 1 A, Fig. 5 J, and Fig. 6 D from Video 5). After anaphase II, MAP65-3 localized in the midzones between the four newly forming nuclei (Fig. 6, C and D from Video 5).

In *VF cdka;1/- cdkd;3/-* mutant plants, MAP65-3 was generally more diffuse than in WT (Fig. 6 E), consistent with the less

organized microtubule pattern in the mutant as described above. At late prophase I, before NEB, bundled microtubules were decorated with MAP65-3, resembling a phragmoplast-like microtubule organization (Fig. 6, E–G, white asterisks). Live-cell imaging revealed that these structures persisted until metaphase I, where they rapidly disappeared and were apparently incorporated into the microtubules forming the meiotic spindle (Fig. 6, H and I from Video 6). Afterward, MAP65-3 localized to the phragmoplast of the terminal cell division after meiosis I observed in *VF cdka;1/- cdkd;3/-* and was removed in an outside-in fashion, consistent with a centripetal formation of the new cell wall (see above).

Taken together, these data show that CDKDs together with CDKA;1 are major regulators of the microtubule cytoskeleton and cytokinesis in meiosis. On the one hand, they appear to be necessary for the proper formation of distinct microtubule structures, such as the half-moon structure in prophase I or the meiotic spindle. On the other hand, they are important for repression of untimely microtubule configurations in prophase I and also prevent cytokinesis after meiosis I. Remarkably, a moderate reduction of CDKA;1 activity and premature cell wall formation is compatible with entry into a second meiotic division, for which sufficient CDKA;1 activity is needed again.

CDKA;1 and TUA5 colocalize at the spindle during metaphase I and II

To explore the dynamics of CDKA;1 with respect to the microtubule cytoskeleton, we combined plants expressing TagRFP:TUA5 with our functional CDKA;1 reporter line (*PRO_{CDKA;1}:CDKA;1:mVenus*; Yang et al., 2020) and with plants expressing *PRO_{CDKA;1}:mVenus* as a negative control. Free mVenus was expected to localize to both the cytoplasm and the nucleus. Although we found this pattern in tapetum cells, mVenus was predominantly localized to the nucleus in meiocytes for unknown reasons. Nonetheless, as described below, the construct could serve as a negative control compared with the CDKA;1:mVenus fusion during the course of meiosis.

We first analyzed a possible colocalization pattern in late prophase I, when microtubules were localized in a ring-like structure around the nucleus (Fig. 7, A and B, first row). The profile plots of signal intensities from a line going through the meiocyte revealed no overlap between free mVenus and tubulin (Fig. 7 C, first panel). Whether CDKA;1:mVenus specifically colocalized with tubulin could not be unambiguously decided, since CDKA;1:mVenus is also strongly present everywhere in the cytoplasm at this stage (Fig. 7 D, first panel). Shortly before NEB, when the microtubule structures start to rearrange to form the first spindle, both free mVenus and the CDKA;1:mVenus fusion protein were still surrounded by microtubules, and like the stage before, a clear colocalization pattern of CDKA;1:mVenus with microtubules could not be unambiguously confirmed (Fig. 7, A and B, second rows).

After NEB, however, when the spindle was fully assembled at metaphase I, CDKA;1:mVenus was enriched in the region of the

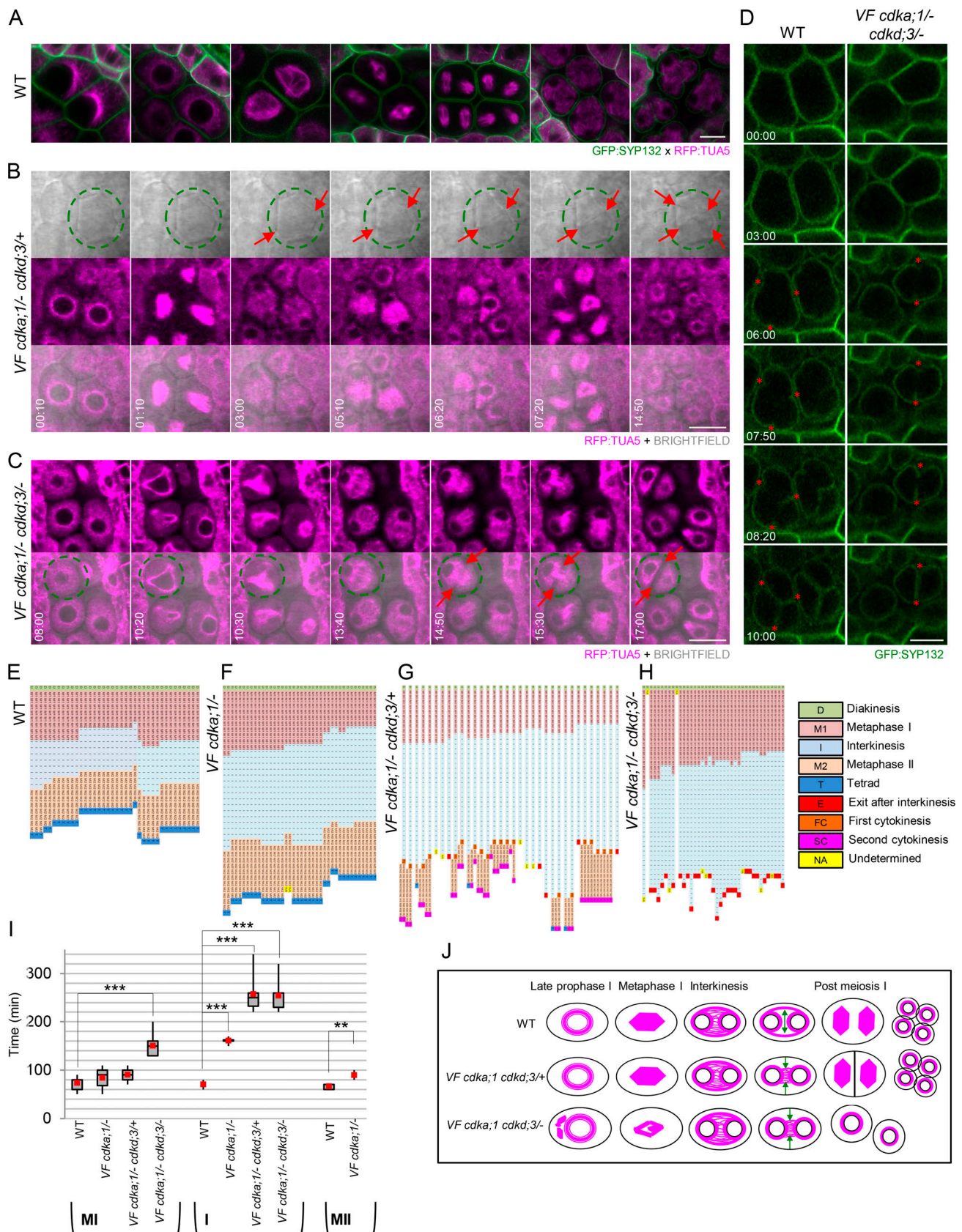


Figure 5. **Analysis of meiotic progression in WT and VF *cdkd;3* mutants.** (A) Confocal laser scanning micrographs of male meiocytes expressing TagRFP: TUA5 (magenta) and GFP:SYN132 (green) during meiotic progression in WT (time indicated with white numbers: h:min). See also Video 1 A. (B) Meiotic progression in VF *cdka;1/- cdkd;3/+* (time indicated with white numbers: h:min) showing the conversion of a simultaneous into a successive cytokinesis in one

male meiocyte highlighted with a green circle (from Video 2). TagRFP:TUA5 in magenta and bright field in gray, overlay in the third row, cell wall deposition is marked with red arrows. **(C)** Meiotic progression in one meiocyte (green circle) of *VF cdka;1/- cdkd;3/-* mutant expressing TagRFP:TUA5 (in magenta) and the respective overlay with the bright field in the second row, showing microtubule dynamics and cell wall deposition (red arrows) from late prophase I to meiotic exit (from Video 3; time indicated with white numbers: h:min). **(D)** Comparison of simultaneous cytokinesis in WT versus meiotic exit in *VF cdka;1/- cdkd;3/-* using GFP:SYP132 (green) as plasma membrane marker (from Video 4). Red asterisks mark the initiation and the outside-in direction of cell wall deposition during cytokinesis; time indicated with white numbers: h:min. **(E–H)** Comparison of the duration of meiotic stages for single meiocytes between WT (E), *VF cdka;1/-* (F), *VF cdka;1/- cdkd;3/+* (G), and *VF cdka;1/- cdkd;3/-* (H). Every line represents a single cell undergoing meiosis, and every square, a 10-min interval of a specific meiotic stage: diakinesis (D), metaphase I (M1), interkinesis (I), metaphase II (M2), and telophase II/tetrad (T). In some mutants, exit after interkinesis (E) or a first cytokinesis (FC) is observed. After the second meiotic division, a second cytokinesis (SC) finally leads to the formation of meiotic products. Data aligned by taking a starting point 10 min before the first meiotic spindle is visible and, as final time point, 10 min after the spindle of the second meiotic division disappears. **(I)** Box plots of metaphase I, interkinesis, and metaphase II duration in WT ($n = 38$), *VF cdka;1/-* ($n = 40$), *VF cdka;1/- cdkd;3/+* ($n = 34$), and *VF cdka;1/- cdkd;3/-* ($n = 37$). Red dots represent the mean value. Level of significance (*, $P < 0.05$; **, $P < 0.01$; ***, $P < 0.001$) determined by one-way ANOVA followed by Tukey's test. **(J)** Cartoons summarizing microtubule organization during meiotic progression in WT versus *VF cdka;1 cdkd;3* mutant combinations. Green arrows represent the direction of microtubule removal in the midzone during late interkinesis. Scale bar in A–D, 10 μm .

spindle microtubules (Fig. 7 B, third row) and the signal intensities overlapped (Fig. 7 D, third panel), whereas the free mVenus signal, albeit weak after NEB (Fig. 7 A, third row), was not found to be enriched at spindle fibers (Fig. 7 C, third panel). Similarly, at metaphase II, both spindles were slightly enriched with CDKA;1:mVenus (Fig. 7 B, last row, and Fig. 7 D, last panel), but not with free mVenus (Fig. 7 A, last row, and Fig. 7 C, last panel). Together with the spindle defects observed before, we conclude that CDKA;1 is an important regulator of the meiotic spindle and likely directly acts on the spindle fibers and/or associated factors, although we cannot rule out that spindle defects are at least partially caused in an indirect manner, e.g., from an effect of low CDKA;1 activity on cortical microtubules.

CYCB3;1 functions together with CDKA;1 to regulate microtubule organization during meiosis

Essential for the activation of CDKA;1 is not only the phosphorylation by CDKDs, but also the binding of a cyclin cofactor. Because a β -glucuronidase (GUS) fusion to CYCB3;1 was previously found to localize to both meiotic spindles, we suspected that CYCB3;1 could be a regulator of MT in meiosis (Bulankova et al., 2013). Previous mutant analyses revealed a function of CYCB3;1 in repressing premature cell wall deposition and ensuring the accuracy of cell wall formation (Bulankova et al., 2013). To address a possible function of CYCB3;1 in microtubule organization, we first monitored root growth of *cycb3;1* mutants on agar plates containing the microtubule-depolymerizing reagent oryzalin. As a positive control, we used mutants in the central spindle assembly checkpoint component *MITOTIC ARREST DEFICIENT 1 (MAD1)*, which are hypersensitive to this drug (Komaki and Schnittger, 2017). Indeed, the growth of *cycb3;1/-* mutants was as strongly reduced as *mad1/-* on oryzalin in comparison with WT, pointing to a function of CYCB3;1 in regulating the microtubule cytoskeleton (Fig. S5 A).

To understand the role of CYCB3;1 during meiosis, we first generated a genomic CYCB3;1 reporter, in which the ORF for GFP was inserted right before the stop codon of CYCB3;1 (*PRO_{CYCB3;1}:CYCB3;1::GFP*). This reporter fully rescued the oryzalin sensitivity of root growth found in *cycb3;1/-* mutants, and we hence conclude that it is functional (Fig. S5 A). CYCB3;1 was then found to accumulate in the cytoplasm of meiocytes throughout prophase I and appeared to be associated with the spindle at metaphase I, while it was not present in metaphase II, in contrast to a previous report (Bulankova et al.,

2013; Fig. 8 A). The spindle localization of CYCB3;1:GFP was confirmed by live-cell imaging in plants coexpressing the *TagRFP:TUA5* reporter (Fig. 8 B from Video 7). Currently, we cannot explain the discrepancy between the previously used GUS fusion with CYCB3;1 that indicated the presence of CYCB3;1 at the second meiotic spindle and our reporter. Possibly, the GUS tag interfered with the degradation of CYCB3;1, making it available when the second meiotic spindle was formed.

To investigate whether CDKA;1 and CYCB3;1 work together in organizing microtubules, we first performed an in vitro pull-down assay using Strep-CDKA;1 and HisMBP-CYCB3;1 (Fig. 8 C), showing clearly an interaction of both proteins. Second, we combined our *VF cdka;1/-* with a *cycb3;1/-* mutant and performed chromosome spreads. In *cycb3;1/-* meiocytes, similar to WT meiosis (Fig. 1 A), chromosomes condensed into five bivalents at metaphase I, correctly segregated to two opposite poles at anaphase I, shortly decondensed at interkinesis before recondensing at metaphase II, and after sister chromatid separation, distributed equally to four pools at telophase II (Fig. 8 D, first row). However, several meiotic defects were observed in *VF cdka;1/- cycb3;1/-* mutants: chromosomes failed to properly align in the metaphase I plane, lagging chromosomes were found in anaphase I and telophase I (Fig. 8 D, second row, red arrows), the organellar band separating the two pools of chromosomes was not correctly positioned or fully missing in interkinesis, and irregular and unbalanced metaphase II chromosome assemblies, likely as a consequence of unequal chromosome segregation in meiosis I, were observed, leading to unbalanced tetrads in 72% of cases (Fig. 8 D, second row). The defective meiotic progression is supported by a high level of pollen abortion and very short siliques in *VF cdka;1/- cycb3;1/-* plants (Fig. S5, B–F).

The introgression of the tubulin marker TagRFP:TUA5 in *VF cdka;1/- cycb3;1/-* plants showed defective spindle structures in metaphase I (Fig. 8 F), whereas *cycb3;1/-* single mutants were characterized by a fully assembled and condensed spindle (Fig. 8 E). Thus, combining *cycb3;1/-* with *VF cdka;1/-* strongly enhanced the *VF cdka;1/-* mutant phenotype, similar to the enhancement found in combinations of *VF cdka;1/-* with *cdkd* mutants. This genetic interaction, together with the physical interaction of CYCB3;1 and CDKA;1, indicates that they build a functional complex in vivo.

To further investigate the regulation of microtubules by CYCB3;1, we developed an in vivo oryzalin treatment assay and monitored meiotic progression using confocal microscopy. Briefly, anthers from WT and *cycb3;1/-* mutant plants expressing

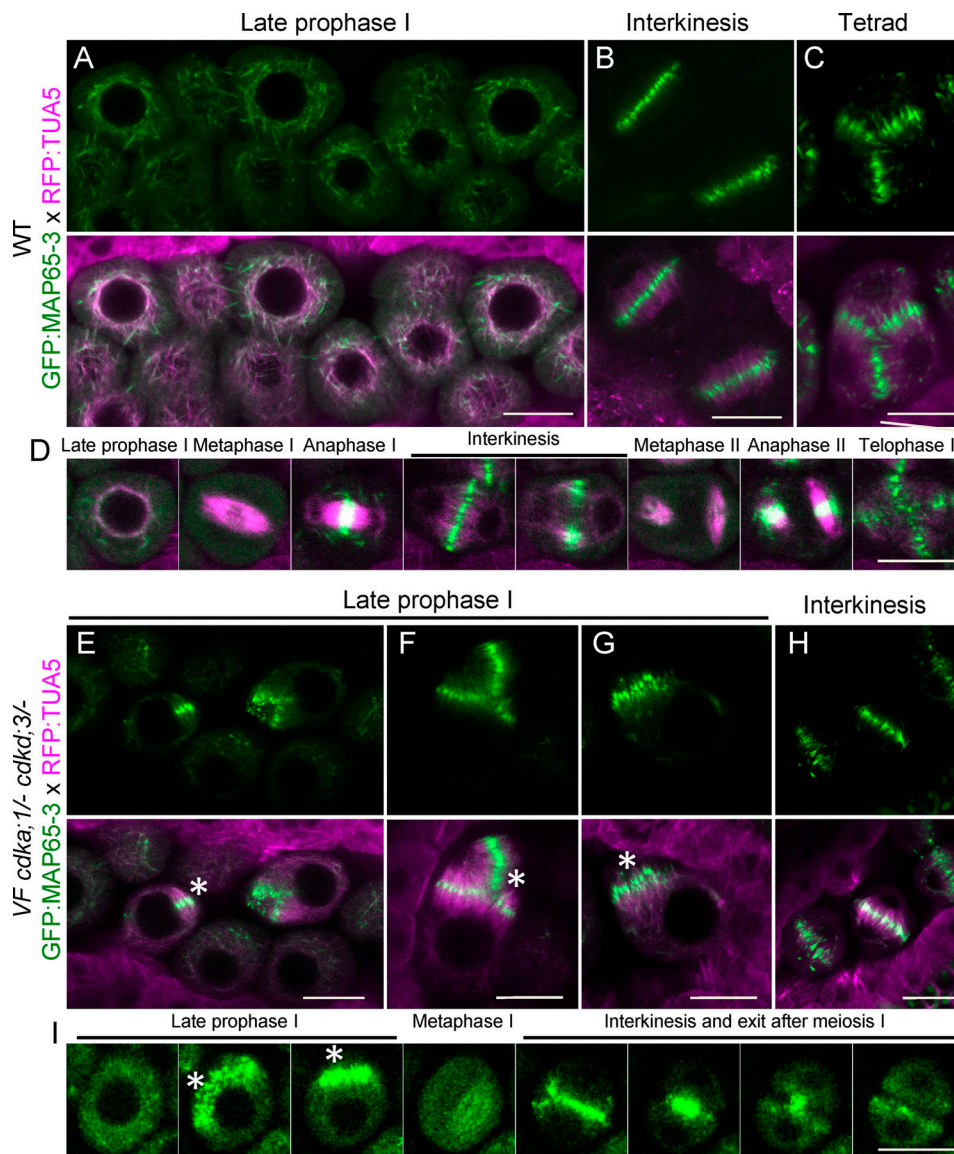


Figure 6. **Formation of premature antiparallel microtubule bundle structures in plants with low CDKA;1 activity.** (A–C) Confocal laser scanning micrographs of meicytes expressing TagRFP:TUA5 (magenta) and GFP:MAP65-3 (green) at late prophase (A), interkinesis (B) and tetrad (C) in WT. (D) Time course of TagRFP:TUA5 and GFP:MAP65-3 from late prophase to telophase II in WT (from Video 5). (E–H) Confocal micrographs of meicytes expressing TagRFP:TUA5 (magenta) and GFP:MAP65-3 (green) at late prophase (E–G) and interkinesis (H) in *VF cdk1;1- cdk3;3-*. (I) Time course of TagRFP:TUA5 and GFP:MAP65-3 from late prophase to exit after meiosis I in *VF cdk1;1- cdk3;3-* (from Video 6). White asterisks highlight antiparallel microtubule bundles. Scale bar, 10 μ m.

TagRFP:TUA5 were simultaneously transferred to plates containing DMSO or oryzalin before time-lapse imaging (Fig. 9 A). On medium containing DMSO as control, meiotic progression from mid-prophase I (half-moon stage) to tetrad formation was indistinguishable between *cycb3;1-* mutants and WT, matching the progression in WT without any treatment as described above (Fig. 9, B and C from Video 8). On medium containing 200 nM oryzalin, WT meicytes also correctly progressed through meiosis (Fig. 9 D from Video 9), while in *cycb3;1-* mutants, microtubule structures were perturbed at late prophase I, and the length of the first meiotic spindle was shorter at metaphase I compared with WT (Fig. 9 E from Video 9 H). Strikingly, microtubule structures in *cycb3;1-* meicytes completely dissolved

on medium containing 500 nM oryzalin shortly after the start of image acquisition, and the two meiotic spindles were never formed. After two events of NEB, unreduced gametes were produced, whereas WT meicytes were still able to form two spindles, with the subsequent appearance of tetrads (Fig. 9, F and G from Video 10, H and I). Taken together, these data suggest a novel role of CYCB3;1 as a CDKA;1 partner in regulating microtubule organization during meiosis.

Discussion

Here, we have analyzed the role of CDKDs as CDKA;1-activating kinases in meiosis. Earlier work indicated that activation of

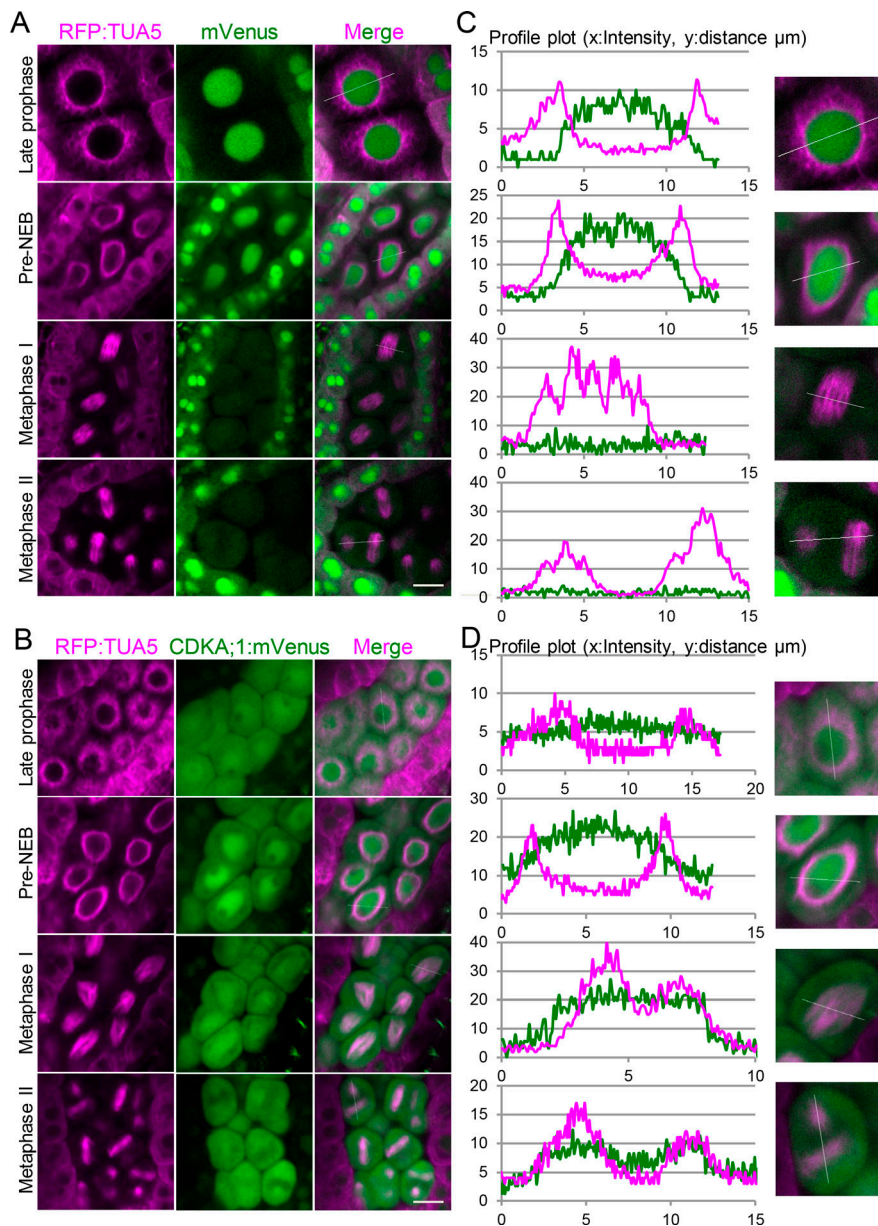


Figure 7. CDKA;1 colocalizes with the spindle in metaphase I and metaphase II. (A) Confocal laser scanning micrographs showing the localization of TagRFP:TUA5 (magenta, first column) expressed from the PRO_{RP55A} promoter and mVenus (green, second column) expressed from the $PRO_{CDKA;1}$ promoter in late prophase, shortly before NEB, metaphase I, and metaphase II. Third column represents the merge of the two channels. (C) Signal intensity plot profile of a section (white line) through one meiocyte shown in A (close-up in second column). (B) Confocal laser scanning micrographs showing the localization of Tag:RFP:TUA5 (magenta, first column) expressed from the PRO_{RP55A} promoter and a CDKA:mVenus (green, second column) fusion proteins expressed from the $PRO_{CDKA;1}$ promoter in late prophase, shortly before NEB, and metaphase I and II. Third column represents the merge of the two channels. (D) Signal intensity plot profile of a section (white line) through one meiocyte (close-up in second column). Scale bar, 10 μ m.

CDKA;1 through T-loop phosphorylation, similar to the regulation of Cdk1-type kinase in other model systems, is crucial for cell division control in mitosis and meiosis in *Arabidopsis* (Harashima et al., 2007; Dissmeyer et al., 2007; Bulankova et al., 2010; Takatsuka et al., 2015). Our genetic experiments and the colocalization data support previous in vitro kinase assays in that this activation is catalyzed by D-type CDKs. Combining mutants in any of the three partially redundantly acting *CDKD* constructs together with a weak loss-of-function mutant in *CDKA;1* gives rise to a very fine-grained genetic reduction of CDKA;1 activity and hence is a powerful tool to dissect the requirement of CDKA;1 action in meiosis.

CDK levels in mitosis versus meiosis

Progression through the mitotic cell cycle is thought to be driven by oscillating levels of CDK activity, leading to a quantitative control system of the cell cycle: i.e., low kinase levels are

required for the licensing of DNA replication, moderate levels to trigger DNA replication, and high levels to execute mitosis, followed by again low levels of kinase activity to exit mitosis and execute cytokinesis, paving the road for a new S-phase (Stern and Nurse, 1996). These events are intriguingly connected by different circuits, for instance successful attachment of all kinetochores with spindle fibers triggers the decline of CDK activity by activating the anaphase-promoting complex/cyclosome (APC/C) that mediates the degradation of the cyclin cofactors (Komaki and Schnittger, 2017).

The concept of quantitative cell cycle control is largely based on experiments in yeast, especially fission yeast, in which a single CDK-cyclin pair has been found to be sufficient to drive progression through the entire mitotic cell cycle (Fisher and Nurse, 1996; Coudreuse and Nurse, 2010; Gutiérrez-Escribano and Nurse, 2015). In multicellular animals, the situation is less clear, since many more CDKs and cyclins are present and appear

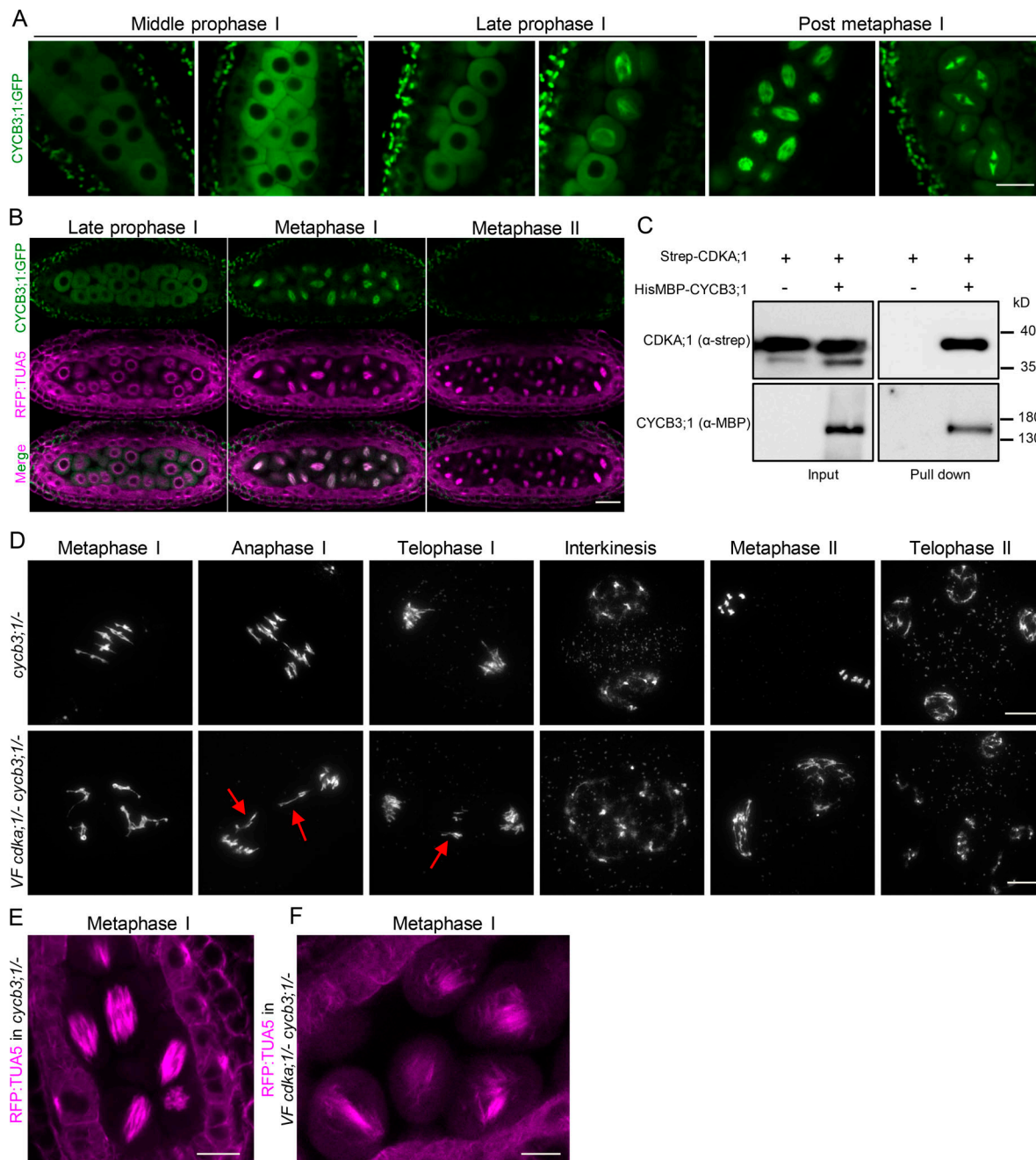


Figure 8. Characterization of CYCB3;1 in meiosis. (A) Confocal laser scanning micrographs showing the localization of a functional reporter for CYCB3;1 (CYCB3;1:GFP in green) throughout meiosis. Scale bar, 10 μ m. (B) Confocal micrographs of TagRFP:TUA5 (magenta) and CYCB3;1:GFP (green) at late prophase I and metaphase I and II (from Video 7). CYCB3;1 colocalizes with the first but not the second spindle. Scale bar, 20 μ m. (C) CYCB3;1 forms a complex with CDKA;1. Pull-down assay using Strep-CDKA;1 in the presence or absence of HisMBP-CYCB3;1. The input and pull-down fractions were detected by immunoblotting with anti-Strep (upper panel) and anti-MBP (lower panel) antibodies. (D) Chromosome spread analysis of *cycb3;1*^{-/-} versus *VF cdk;1*^{-/-} *cycb3;1*^{-/-} during metaphase I, anaphase I, telophase I, interkinesis, metaphase II, and telophase II. Red arrows mark lagging chromosomes at anaphase I and telophase I. Scale bar, 10 μ m. (E and F) Confocal laser scanning micrographs of TagRFP:TUA5 during metaphase I in *cycb3;1*^{-/-} (E) and *VF cdk;1*^{-/-} *cycb3;1*^{-/-} (F). Microtubule arrays are altered in *VF cdk;1*^{-/-} *cycb3;1*^{-/-} as represented by irregular spindles at metaphase I. Scale bar, 10 μ m.

to be required for a development-specific regulation of the cell cycle (Pagliuca et al., 2011). Nonetheless, all CDKs but Cdk1 are dispensable in mice (Santamaría et al., 2007). Moreover, in *Arabidopsis*, even the Cdk1 ortholog CDKA;1 is not essential to drive cell division (Nowack et al., 2012), suggesting that a quantitative rather than a qualitative model of cell cycle

regulation is, at least in part, at the heart of the cell cycle of multicellular eukaryotes, too.

The control of progression through meiosis is particularly complex, since a single DNA replication phase is followed by two chromosome separation events. Largely based on experiments in yeast, it has been proposed that CDK activity after anaphase I

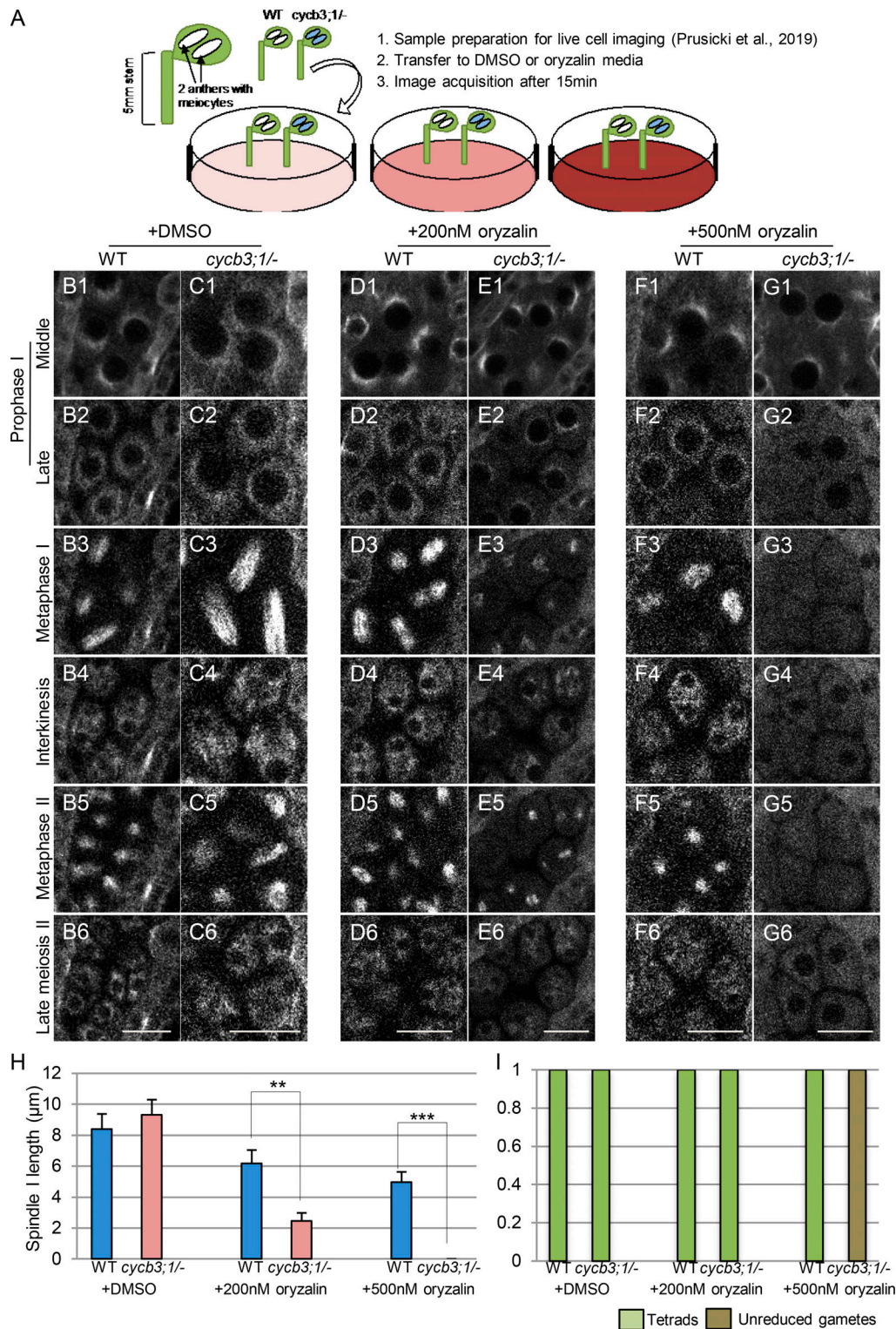


Figure 9. **Meiocytes of *cycb3;1-* mutants are hypersensitive to oryzalin.** (A) Scheme of live-cell imaging of male meiocytes treated with oryzalin. (B–G) Time points of meiotic progression in meiocytes expressing TagRFP:TUA5 in WT (B1–B6) and *cycb3;1-* (C1–C6) with DMSO (from Video 8); WT (D1–D6) and *cycb3;1-* (E1–E6) with 200 nM oryzalin (from Video 9); and WT (F1–F6) and *cycb3;1-* (G1–G6) with 500 nM oryzalin (from Video 10). Scale bar, 10 µm. (H) Spindle length at metaphase I of meiocytes from at least three different anthers of WT ($n = 28$) and *cycb3;1-* ($n = 23$) treated with DMSO; WT ($n = 22$) and *cycb3;1-* ($n = 25$) treated with 200 nM oryzalin; and WT ($n = 23$) and *cycb3;1-* ($n = 20$) treated with 500 nM oryzalin. Level of significance (*, $P < 0.05$; **, $P < 0.01$; ***, $P < 0.001$) determined by one-way ANOVA followed by Tukey’s test. (I) Number of meiotic products (tetrads or unreduced gametes) of meiocytes from at least three different anthers of WT ($n = 28$) and *cycb3;1-* ($n = 23$) treated with DMSO; WT ($n = 22$) and *cycb3;1-* ($n = 25$) treated with 200 nM oryzalin; and WT ($n = 23$) and *cycb3;1-* ($n = 20$) treated with 500 nM oryzalin.

drops owing to the activation of the APC/C but is not fully eliminated. This residual level of CDK activity is important to prevent the initiation of another S-phase and to trigger the second meiotic division (Pesin and Orr-Weaver, 2008). Consistent with this model, APC/C inhibitors have been identified in different model systems, including *Arabidopsis*, that prevent the full activation of the APC/C and hence the complete loss of CDK activity (Pesin and Orr-Weaver, 2008). Accordingly, mutants in the APC/C inhibitor *OSDI/GIG1* resulted in the termination of meiosis after the first division in *Arabidopsis* (d'Erfurth et al., 2009). Likewise, mutants in the meiotic cyclin *TAM* exit meiosis after meiosis I (Magnard et al., 2001; Wang et al., 2004b; d'Erfurth et al., 2010; Bulankova et al., 2010), and as detailed in this study, strong reduction of CDK activity also results in exit of meiosis after the first meiotic division.

We currently cannot exclude that the meiotic defects seen in plants with low kinase activity could be indirectly caused by defects in the neighboring tissue, i.e., tapetum cells. Indeed, defects in the tapetum layer can affect the differentiation of male meiocytes and/or the progression through meiosis, often through the action of small RNAs that are produced outside of meiocytes (Lei and Liu, 2020). Defects in cytokinesis of meiocytes have been reported when the signaling pathway of the plant hormone gibberellic acid (GA) was disturbed by exogenous application of GA or in double mutants for the GA-signaling repressors *GAI* (GA insensitive) and *RGA* (repressor of *GAI-3*), which function as transcriptional repressors (Liu et al., 2017). Interestingly, an *RGA* reporter construct revealed that this *DELLA* protein is largely absent in meiocytes but accumulated in the surrounding cells, including tapetum cells. While the expression pattern of *GAI* in anthers has not been revealed, this result hints at a possible non-cell-autonomous function of GA signaling controlling cytokinesis in meiocytes (Liu et al., 2017).

However, the cytokinesis defects seen in plants with reduced *CDKA;1* activity do not resemble the effects after application of GA, as for instance triads are predominantly formed when the GA pathway is perturbed, but not in mutants with reduced *CDKA;1* activity. We also did not find any obvious hints for defective tapetum cells. In addition, so far none of the mutants with defects in tapetum cells has been found to cause the formation of univalents or affect other aspects of chromosomal dynamics in prophase I as observed here (Lei and Liu, 2020). Consistently, live-cell imaging of chromosome dynamics in male meiocytes also suggested that chromosome behavior in meiosis progresses rather independently from the differentiation of tapetal cells (Prusicki et al., 2019). Moreover, the termination of meiosis and the formation of ectopic phragmoplast-like structures in plants with low *CDKA;1* activity resemble the defects seen in *tam* mutants (Magnard et al., 2001; Wang et al., 2004b; d'Erfurth et al., 2010; Bulankova et al., 2010; Prusicki et al., 2019). *TAM* encodes for a cyclin, which forms active complexes with *CDKA;1* and is not present in tapetal cells (Wang et al., 2004b; Bulankova et al., 2010; Cifuentes et al., 2016). These data, together with the accumulation pattern of *CDKA;1* and *CDKDs* in meiocytes (this study and (Bulankova et al., 2010)), suggest a cell-autonomous role of *CDKA;1* in meiosis.

Unexpectedly, we found here that a moderate reduction of CDK activity was enough to trigger cytokinesis but did not

necessarily lead to termination of meiosis in male meiocytes as previously observed in *tam* and *osdl/gig* mutants (Magnard et al., 2001; Wang et al., 2004b; d'Erfurth et al., 2009, 2010; Bulankova et al., 2010; Prusicki et al., 2019). Instead, a second meiotic division was executed, resulting in four spores as in WT. This result is surprising, since cell cycle regulators are usually interconnected to generate bistable switches in which both the high and the low activity levels are reinforced by positive feedback loops (Tyson and Novák, 2015). In contrast, we observed a rather gradual, yet apparently stable, response to high, moderate, and low levels of CDK activity. This gives rise to the speculation that some of the feedback mechanisms of mitosis are not implemented in meiosis. Interestingly, it has been found that meiosis requires much higher kinase levels than mitosis, possibly because of lower affinities of CDKs for meiotic substrates and/or the requirement of high levels of phosphorylation of meiotic substrates (Gutiérrez-Escribano and Nurse, 2015). Our findings now offer an additional reason: If reinforcement circuits are not present or are less active in meiosis, higher CDK levels might be needed to promote meiosis. In turn, the possible absence of these reinforcement circuits might be necessary to prevent the complete loss of CDK activity after meiosis I.

CDKA;1: A master regulator of meiosis?

It is well established that *Cdk1* is a master regulator of mitosis that controls many different processes, and several hundred possible *Cdk1* substrates have been identified from yeast to plants (Ubersax et al., 2003; Holt et al., 2009; Van Leene et al., 2010; Pusch et al., 2012). The role of *Cdks* in meiosis is less understood, possibly owing to the requirement of *Cdk1* for somatic/sporophytic development of multicellular organisms, making a functional analysis of *Cdk1* action in meiosis challenging. In addition, several other kinases have been found in yeast and animals to be important for meiotic entry and progression, including *Cdk2* (Ortega et al., 2003). However, in an analysis of conditional *Cdk1* knockout mice, it was demonstrated that *Cdk1* is essential for meiosis in mammalian oocytes (Adhikari et al., 2012). Moreover, *Cdk1* function in meiosis cannot be substituted by *Cdk2* (Satyanarayana et al., 2008). In parallel, several meiotic proteins have been found to be phosphorylated by *Cdks*. These include *Mer2/Rec107* (meiotic recombination 2 or recombination 107), which is important for double-strand break formation (Henderson et al., 2006), and *Sae2/Com1* (sporulation in the absence of *Spo11* or completion of meiotic recombination), a nuclease that is important to process double-strand breaks (Huertas et al., 2008).

In plants, the *Cdk1* orthologue *CDKA;1* has been found to control meiotic progression, cohesion of sister chromatids, formation of the chromosome axis, and crossover number and placement (Dissmeyer et al., 2007; Yang et al., 2019; Wijnker et al., 2019). Possible substrates are the chromosome axis-associated protein *ASYNAPTIC 1*, the putative APC/C inhibitor *THREE DIVISION MUTANT 1* (*TDM1*), the endonuclease *MutL* homolog 1, and *switch1/dyad*, a novel repressor of the cohesin remodeling factor *WINGS APART LIKE* (Cifuentes et al., 2016; Wijnker et al., 2019; Yang et al., 2019, 2020). The list of putative substrates of *CDKA;1* in meiosis is very long and includes further

key proteins involved in all aspects of meiosis, e.g., ZYP1 (zipper 1), a protein of the central region of the synaptonemal complex, which harbors many CDKA;1 consensus phosphorylation sites.

Here, we have assigned a new role to CDKA;1, i.e., the regulation of microtubule organization in meiosis. Interestingly, CDKA;1 is needed for different aspects of microtubule dynamics, which include foremost the organization of the meiotic spindle and the repression of a premature/ectopic phragmoplast-like structure. An antagonist relationship between CDK activity and cytokinesis has been found in mitosis. A mitosis-specific B-type CDK was found to phosphorylate and inhibit the function of NACK1 (NPK1-activating kinesin 1), a kinesin, and Nicotiana protein kinase 1 (NPK1), a MAP3K, in *Arabidopsis*. By that, a mitotic CDK prevents that NACK1 together with NPK1 triggers a MAP kinase phosphorylation cascade that results in the activation of MAP65-3 and subsequent cytokinesis (Sasabe et al., 2011).

Whether CDKA;1 targets the same cytokinesis regulators in meiosis is not clear at the moment and awaits further studies. In addition, CDKA;1 likely has many more targets in regulating the microtubule organization in meiosis. One of them could be MAP65-3 itself, which has three predicted CDK phosphorylation sites. Interestingly, the human MAP65-1 homologue, PRC1, which has a redundant function with MAP65-3, shows decreased MT bundling activity upon phosphorylation by Cdk1 and Cdk2 complexes (Jiang et al., 1998; Mollinari et al., 2002). Consistent with a possible regulation of MAP65-3 by CDKA;1, we found that MAP65-3 localization is more diffuse in mutants with reduced CDKA;1 activity than that in WT. Thus, although we could show the importance for CDKA;1 activity for proper timing and organization of spindle and phragmoplast microtubules in meiosis, additional work is needed to identify and characterize the phospho-targets of CDKA;1 involved in these processes.

Modulation of CDK activity to dissect the regulation of cytokinesis

Most cytokinetic events in multicellular land plants follow an inside-out modus, i.e., a phragmoplast starts to be assembled in the middle of the division plane and then expands laterally (Müller and Jürgens, 2016; De Storme and Geelen, 2013).

The here-observed conversion of a simultaneous into a successive cytokinesis without a concomitant change of the outside-in to an inside-out modus shows that the type of cytokinesis in *Arabidopsis* is not strictly coupled to the mode of cell wall deposition. This is in accordance with observation in monocotyledonous species, in which cytokinesis in male meiosis follows the inside-out strategy in not only species that go through successive cytokinesis (De Storme and Geelen, 2013), but also species that undergo simultaneous cytokinesis (Ressayre et al., 2005). It is interesting to note that, while the timing of division is under control of CDK activity, the type of cell division mode seems to be dependent on the developmental state of the mother cell. The termination of meiosis with the formation of a cell wall after meiosis I in a *tam* mutant has been regarded as a partially successive cytokinesis, and staining of the cell wall component callose has suggested that cell wall formation follows an outside-in pattern (Magnard et al., 2001; Albert et al., 2011).

The defects in *tam* are consistent with TAM being a cyclin partner for CDKA;1 and are furthermore in accordance with the idea that CDKA;1-TAM complexes control phragmoplast formation as described here and in Prusicki et al. (2019). Interestingly, *tam* does not appear to affect the meiotic spindle (Bulankova et al., 2010; Prusicki et al., 2019), and CDKA;1 together with CYCB3;1, and likely additional cyclins, regulate spindle microtubules as shown here.

Coupled with the question of whether a successive versus simultaneous cytokinesis is executed is how the geometry of cell division is controlled. Is the reorientation of the second spindle that leads to a tetrahedral organization of the male meiotic products due to some preset landmarks in the male meiocyte that are read out at the duration of first division, or is it de novo established after the first division? The analysis presented here and previous work on a hypomorphic *tam* mutant, in which a second meiotic division occasionally takes place (Magnard et al., 2001; Albert et al., 2011), indicate that the reorientation of the second spindle is likely established after the first division and does not use any cues present in the male meiocyte before cytokinesis (Albert et al., 2011). Thus, the first spindle itself likely influences directly or indirectly the orientation of the second spindle. It will now be interesting to explore how such cross-talk could be molecularly realized.

Materials and methods

Plant material and growth conditions

The *Arabidopsis thaliana* accession Columbia (Col-0) was used as WT reference for this study. The transfer DNA insertion lines SALK_106809 (*cdka;1*; Nowack et al., 2006) MPI_8258 (*cdkd;1-1*), SALK_065163 (*cdkd;2-1*), SALK_120536 (*cdkd;3-1*; Shimotohno et al., 2006; Hajheidari et al., 2012), and WiscDsLox461-464II0 (*cycb3;1-1*; Bulankova et al., 2013) were obtained from the SALK SIGNAL, GABI-Kat, and WISC transfer DNA mutant collections. All genotypes were determined by PCR using the primers shown in Table S1. The mutants *PRO_{CDKA;1}:CDKA;1^{T14V;Y15F}* as well as *PRO_{CDKA;1}:CDKA;1^{T16ID}* and the reporter lines KINGBIRD2 (*PRO_{REC8}:REC8:GFPxPRO_{RPS5A}TagRFP:TUA5*), *PRO_{CDKA;1}:CDKA;1:mVenus*, *PRO_{RPS5A}TagRFP:TUA5*, and *PRO_{SYPI32}GFP:SYPI32* were previously described (Dissmeyer et al., 2007, 2009; Prusicki et al., 2019; Park et al., 2018; Enami et al., 2009; Yang et al., 2020). All seeds were surface sterilized with chloride gas, sown on 1% agar plates containing 1/2 Murashige and Skoog salts and 1% sucrose, pH 5.8. Hygromycin B (25 mg/l; Duchefa Biochemie) was used for seed selection. Seeds were germinated on plates in long-day conditions (16-h day/8-h night at 22°C/18°C; 7 d) and then transferred to soil. After a 2-wk period under short-day conditions (12-h day/12-h night), plants were grown in long-day conditions with 60% humidity until seed production.

Plasmid construction and plant transformation

To generate the *PRO_{CDKD}:CDKD:mVenus* reporters, a genomic fragment of *CDKD;1*, *CDKD;2*, and *CDKD;3* from 1,697, 2,011, and 2,000 bp upstream of the start codon to 994, 118, and 1,000 bp downstream of the stop codon was amplified by PCR, respectively, and cloned into the gateway entry vector *pDONR221*

(Invitrogen). Then, *mVenus* fragments amplified by PCR were cloned into the vectors by conducting In-Fusion Cloning (Clontech). In each case, the *mVenus* tag was inserted directly before the STOP codon. A Gateway LR reaction (Invitrogen) was used to transfer the genomic *PRO_{CDKD}:CDKD:mVenus* fusions into the destination vector *pGWB1* (Nakagawa et al., 2007). For the *PRO_{CDKA;1}:CDKA;1:mVenus* reporter, a 6,210-bp genomic sequence containing the presumptive promoter and 3' UTR regions, and for the *PRO_{CDKA;1}:mVenus*, reporter, a 2,000-bp genomic sequence of the presumptive *CDKA;1* reporter, were amplified by PCR and subsequently integrated into the *pENTR2B* vector by SLICE (seamless ligation cloning extract) reaction. A *SmaI* restriction site was then introduced directly before the stop codon. After linearization by *SmaI* restriction, the constructs were ligated with *mTurquoise2* or *mVenus* fragments, followed by a Gateway LR reaction with the destination vector *pGWB501*. To generate *PRO_{MAP65-3}:GFP:MAP65-3* reporter, the genomic sequence of *MAP65-3* was amplified by PCR with primers flanking the *attB* recombination sites and subcloned into *pDONR221* vector using the Gateway BP reaction. A *SmaI* restriction site was then introduced directly before the start codon. After linearization by *SmaI* restriction, the construct was ligated with the GFP fragment, followed by a Gateway LR reaction with the destination vector *pGWB601*. To generate the *PRO_{CYCB3;1}:CYCB3;1:GFP* reporter, the genomic sequence of *CYCB3;1* was amplified by PCR with primers flanking the *attB* recombination sites and subcloned into *pDONR221* vector using the Gateway BP reaction. The resulting *CYCB3;1* expression cassette was then integrated into the destination vector *pGWB504* harboring a C-terminal GFP tag by the Gateway LR reaction. Transgenic *Arabidopsis* plants were generated using the *Agrobacterium tumefaciens* strain *GV3101* (*pMP90*). A 100-ml overnight culture of *Agrobacterium* harboring these constructs was pelleted and resuspended in a solution containing 5% sucrose and 0.02% Silwet L-77, and plants were transformed by floral dip. The *VFD* construct was generated by site-directed mutagenesis using PfuTurbo polymerase (Stratagene) with *CDKA;1* VF variant (Dissmeyer et al., 2009) as template, and primers similar to those used to generate *CDKA;1-T161D* (Dissmeyer et al., 2007). The *CDKA;1* sequence was flanked by Gateway *attB1* and *attB2* sites and recombined in *pDONR201* (Invitrogen). After sequencing, the obtained gateway entry clones were recombined with the binary gateway destination vector *pAM-PAT-GW-ProCDKA;1*. Resulting expression vectors conferring phosphinothricin resistance were retransformed into *A. tumefaciens* *GV3101-pMP90RK* and transformed into heterozygous *cdka;1/+* by floral dip.

Phenotypic evaluation

To test for potential meiotic abnormalities the following analyses were performed. Pollen size and viability were analyzed by Peterson staining as described previously (Peterson et al., 2010). For pollen analysis, three mature flower buds containing dehiscent anthers were dipped in 15 μ l of Peterson staining solution (10% ethanol, 0.01% malachite green, 25% glycerol, 0.05% fuchsin, 0.005% orange G, and 4% glacial acetic acid) and incubated overnight at room temperature. Similarly, for anther staining, five nondehiscent anthers were

dissected and immersed in 50 μ l of Peterson staining and incubated overnight. Slides were heated at 80°C for 30 min before light-microscope observation.

Cytogenetic analyses were performed via cell spreads as described in Ross et al. (1996). In brief, fresh flower buds were fixed in 3:1 ethanol/acetic acid (fixative solution) for \geq 48 h at 4°C, washed two times with fresh fixative solution, and stored for further use in 70% ethanol at 4°C. Before chromosome spreading, the entire flower buds were digested in 10 mM citrate buffer containing 1.5% cellulose, 1.5% pectolyase, and 1.5% cytohelicase for 3 h at 37°C. Single flower buds were transferred onto a glass slide and squashed with a bended needle for 1 min in 12 μ l of 45% acetic acid. Spreading was performed on a 48°C hot plate for 2 min, and the slide was washed afterward with the fixative solution. After overnight incubation at 37°C, slides were mounted in Vectashield with DAPI (Vector Laboratories).

Live imaging of meiotic progression

Live-cell imaging was performed using the same protocol and sample preparation as described by Prusicki et al. (2019). Up to 10 samples including WT control next to the mutants were followed in the same Petri dish. A W-plan-Apochromat 40 \times /1.0 differential interference contrast water-immersion objective on a Zeiss LSM880 confocal microscope with Zen 2.3 SP1 software (Carl Zeiss) permitted the time-lapse acquisition. *mTurquoise2* was excited at λ 458 nm and detected at λ 460–510 nm; GFP was excited at 488 nm and detected at 495–560 nm; *mVenus* was excited at 514 nm and detected 520–620 nm; and TagRFP was excited at 561 nm and detected at 570–650 nm. Time lapses were acquired as series of eight Z-stacks with 4- μ m intervals (step size) using fluorescence autofocusing. Acquisitions were performed at 18°C. Image drift on Z plane was corrected manually using the review multidimensional data option on Metamorph v7.8. Image drift on XY plane was corrected using the Stack Reg plugin (Rigid Body option) of Fiji.

Oryzalin treatment

A stock solution of oryzalin at a concentration of 100 mM (Duchefa Biochemie) in DMSO was prepared and kept at –20°C. Plates containing oryzalin for live-cell imaging were prepared as described previously (Prusicki et al., 2019). The final concentration of DMSO in the medium was 0.05%. The flower buds together with 5-mm stems from four WT and four mutant plants were transferred simultaneously into the oryzalin or DMSO control plates. The time-lapse acquisition started 15 min after transfer to the plates, and only the anthers containing meiocytes having the microtubule half-moon configuration (middle prophase) were kept for further imaging. For quantification of root growth, 9-d-old seedlings grown on plates with and without oryzalin were photographed, and the primary root length was measured with ImageJ (National Institutes of Health).

Quantification of the duration of the meiotic phases

For quantification of the duration of the meiotic phases from diakinesis to telophase II/tetrad stage, cells were assigned manually by taking a starting point 10 min before the spindle I was visible until tetrad or eventually dyad formation. Data were

collected from meiocytes located in at least four different anthers from different plants of the same genotype.

Colocalization analyses

For the pixel intensity plot, the pixel brightness through a region of interest was measured using ImageJ and plotted against the X dimension. The colocalized pixel map and scatter plot were calculated using the Coloc2 plugin in ImageJ.

Kinase and pull-down assays

To generate the expression construct for HisMBP-CYCB3;1, the full-length coding sequence of CYCB3;1 was amplified by PCR from a cDNA library for Col-0 WT plants with primers flanking *attB* recombination sites and subsequently subcloned into *pDONR223* vector by gateway BP reaction (Table S1). The resulting construct was then integrated into the protein expression vector *pHMGWA* by gateway LR reaction. The Strep-CDKA;1 expression construct was generated previously (Harashima and Schnittger, 2012).

To perform the pull-down assay, bacteria of BL21(DE3)pLysS strain harboring either both HisMBP-CYCB3;1 and Strep-CDKA;1 vectors or only the Strep-CDKA;1 vector, used as control, were generated by the heat shock transformation. Bacteria lysate from 50 ml IPTG-induced bacteria were subjected to the pull-down experiment using Ni-NTA agarose (Qiagen) as the binding matrix. After 1-h incubation, Ni-NTA agarose were washed four times and then boiled quickly in 2× SDS-PAGE sample buffer. The eluted proteins were analyzed by Western blot using antibodies against MBP (New England Biolabs, E8032S) and Strep (Sigma-Aldrich, 71590-M).

Kinase assays with precipitated kinases from plant extracts of transgenic lines were performed as previously described (Dissmeyer et al., 2007). Loading of CDKA;1 variants was shown using a rabbit polyclonal epitope antibody directed against the conserved α -PSTAIRES motif of Cdk2 (Cdc2 p34 [PSTAIRES]: sc-53, Santa Cruz Biotechnology).

Statistical analysis

To evaluate the significance of the differences between genotypes, Student's *t* test was used. The significance of differences between more than two groups was calculated using the ANOVA one-way, followed by Tukey's test. *, $P < 0.05$; **, $P < 0.01$; and ***, $P < 0.001$. The numbers of samples are indicated in the figure legends.

Online supplemental material

Fig. S1 shows the functionality of *CDKD;1*, *CDKD;2*, *CDKD;3*, and *CDKA;1* reporter lines used in this study as they fully complement the *cdk1;1/- cdk2;3/-*, *cdk2;2/- cdk2;3/-*, and *cdka;1/-* mutant phenotypes. Fig. S2 shows the expression pattern and colocalization level of *CDKA;1* and *CDKD;3* throughout meiosis as well as the localization pattern of *CDKD;1* and *CDKD;2* in *Arabidopsis* anthers. Fig. S3 shows the chromosome spreads of single and double *cdk* mutants and *CDKD;1* reporter used in this study. Fig. S4 shows the phenotypic characterization of *VF cdk1;1/- cdk2;3* mutants, i.e., seed abortion, pollen viability, and pollen size together with the meiotic stage repartition and chromosome

spreads analysis of *VF cdk1;1/- cdk2;1* mutants. Fig. S5 shows root growth assay of WT, *CYCB3;1* reporter, and *cyb3;1/-* and *mad1/-* mutants under oryzalin treatment as well as phenotypical analyses i.e., seed abortion and pollen viability of *VF cdk1;1/- cyb3;1/-* mutant compared with WT and single *cyb3;1/-* mutant. Table S1 shows the list of primers used in this study. Video 1 shows microtubule dynamics from late prophase to tetrad formation in WT (A) and *VF cdk1;1/-*. (B). Video 2 shows microtubule dynamics during successive cytokinesis in *VF cdk1;1/- cdk2;3/+*. Video 3 highlights microtubule dynamics during meiotic exit in *VF cdk1;1/- cld3;3/-*. Video 4 shows plasma membrane dynamics during meiotic exit in *VF cdk1;1/- cdk2;3/-* compared with WT. Video 5 shows MAP65-3 dynamics during meiosis in WT. Video 6 highlights the differences of MAP65-3 dynamics between WT and *VF cdk1;1/- cdk2;3/-*. Video 7 shows the localization of *CYCB3;1* from late prophase to telophase II. Video 8 shows microtubule dynamics from mid-prophase to tetrad formation in WT and *cyb3;1/-* in medium containing DMSO only. Video 9 shows microtubule dynamics from mid-prophase to tetrad formation in WT and *cyb3;1/-* in medium containing 200 nM oryzalin. Video 10 shows microtubule dynamics from mid-prophase to gamete formation in WT and *cyb3;1/-* in medium containing 500 nM oryzalin.

Acknowledgments

We are grateful to Dr. Maren Heese (University of Hamburg) for critical reading and helpful comments on the manuscript.

This work was funded by the Ministry of Education, Culture, Sports, Science and Technology KAKENHI (grants 17H06470 and 17H06477) to M. Umeda, a grant for Basic Science Research Projects from the Sumitomo Foundation (180428) to S. Komaki, and a Human Frontier Science Program grant (RGPO023/2018) to A. Schnittger, as well as core funding of Universität Hamburg to A. Schnittger.

The authors declare no competing financial interests.

Author contributions: K. Sofroni, M. Umeda, Y. Hamamura, and A. Schnittger conceived and designed the experiments. K. Sofroni, H. Takatsuka, C. Yang, S. Komaki, L. Böttger, and N. Dissmeyer performed the experiments. M. Umeda and A. Schnittger contributed material and reagents. K. Sofroni, M. Umeda, and A. Schnittger analyzed the data. K. Sofroni, M. Umeda, and A. Schnittger wrote the article.

Submitted: 4 July 2019

Revised: 17 February 2020

Accepted: 4 May 2020

References

- Adhikari, D., W. Zheng, Y. Shen, N. Gorre, Y. Ning, G. Halet, P. Kaldis, and K. Liu. 2012. Cdk1, but not Cdk2, is the sole Cdk that is essential and sufficient to drive resumption of meiosis in mouse oocytes. *Hum. Mol. Genet.* 21:2476–2484. <https://doi.org/10.1093/hmg/dds061>
- Albert, B., C. Raquin, M. Prigent, S. Nadot, F. Brisset, M. Yang, and A. Ressayre. 2011. Successive microsporogenesis affects pollen aperture pattern in the tam mutant of *Arabidopsis thaliana*. *Ann. Bot.* 107: 1421–1426. <https://doi.org/10.1093/aob/mcr074>

- Azumi, Y., D. Liu, D. Zhao, W. Li, G. Wang, Y. Hu, and H. Ma. 2002. Homolog interaction during meiotic prophase I in *Arabidopsis* requires the SOLO DANCERS gene encoding a novel cyclin-like protein. *EMBO J.* 21: 3081–3095. <https://doi.org/10.1093/emboj/cdf285>
- Binarová, P., J. Doležel, P. Draber, E. Heberle-Bors, M. Strnad, and L. Bögre. 1998. Treatment of *Vicia faba* root tip cells with specific inhibitors to cyclin-dependent kinases leads to abnormal spindle formation. *Plant J.* 16:697–707. <https://doi.org/10.1046/j.1365-313x.1998.00340.x>
- Bulankova, P., S. Akimcheva, N. Fellner, and K. Riha. 2013. Identification of *Arabidopsis* meiotic cyclins reveals functional diversification among plant cyclin genes. *PLoS Genet.* 9: e1003508. <https://doi.org/10.1371/journal.pgen.1003508>
- Bulankova, P., N. Riehs-Kearnan, M.K. Nowack, A. Schnittger, and K. Riha. 2010. Meiotic progression in *Arabidopsis* is governed by complex regulatory interactions between SMG7, TDM1, and the meiosis I-specific cyclin TAM. *Plant Cell.* 22:3791–3803. <https://doi.org/10.1105/tpc.110.078378>
- Christophorou, N., T. Rubin, I. Bonnet, T. Piolot, M. Arnaud, and J.-R. Huynh. 2015. Microtubule-driven nuclear rotations promote meiotic chromosome dynamics. *Nat. Cell Biol.* 17:1388–1400. <https://doi.org/10.1038/ncb3249>
- Cifuentes, M., S. Jolivet, L. Cromer, H. Harashima, P. Bulankova, C. Renne, W. Crismani, Y. Nomura, H. Nakagami, K. Sugimoto, et al. 2016. TDM1 Regulation Determines the Number of Meiotic Divisions. *PLoS Genet.* 12: e1005856. <https://doi.org/10.1371/journal.pgen.1005856>
- Colasanti, J., S.O. Cho, S. Wick, and V. Sundaresan. 1993. Localization of the Functional p34cdc2 Homolog of Maize in Root Tip and Stomatal Complex Cells: Association with Predicted Division Sites. *Plant Cell.* 5: 1101–1111. <https://doi.org/10.2307/3869630>
- Coudreux, D., and P. Nurse. 2010. Driving the cell cycle with a minimal CDK control network. *Nature.* 468:1074–1079. <https://doi.org/10.1038/nature09543>
- Cromer, L., J. Heyman, S. Touati, H. Harashima, E. Araou, C. Girard, C. Horlow, K. Wassmann, A. Schnittger, L. De Veylder, et al. 2012. OSD1 promotes meiotic progression via APC/C inhibition and forms a regulatory network with TDM and CYCA1;2/TAM. *PLoS Genet.* 8: e1002865. <https://doi.org/10.1371/journal.pgen.1002865>
- d'Erfurth, I., L. Cromer, S. Jolivet, C. Girard, C. Horlow, Y. Sun, J.P.C. To, L.E. Berchowitz, G.P. Copenhaver, and R. Mercier. 2010. The cyclin-A CYCA1;2/TAM is required for the meiosis I to meiosis II transition and cooperates with OSD1 for the prophase to first meiotic division transition. *PLoS Genet.* 6: e1000989. <https://doi.org/10.1371/journal.pgen.1000989>
- d'Erfurth, I., S. Jolivet, N. Froger, O. Catrice, M. Novatchkova, and R. Mercier. 2009. Turning meiosis into mitosis. *PLoS Biol.* 7: e1000124. <https://doi.org/10.1371/journal.pbio.1000124>
- De Storme, N., and D. Geelen. 2013. Cytokinesis in plant male meiosis. *Plant Signal. Behav.* 8: e23394. <https://doi.org/10.4161/psb.23394>
- De Storme, N., M.C. Van Labeke, and D. Geelen. 2007. Formation of unreduced pollen in *Arabidopsis thaliana*. *Commun. Agric. Appl. Biol. Sci.* 72: 159–163.
- DeLuca, K.F., A. Meppelink, A.J. Broad, J.E. Mick, O.B. Peersen, S. Pektas, S.M.A. Lens, and J.G. DeLuca. 2018. Aurora A kinase phosphorylates Hec1 to regulate metaphase kinetochore-microtubule dynamics. *J. Cell Biol.* 217:163–177. <https://doi.org/10.1083/jcb.201707160>
- Ding, D.Q., Y. Chikashige, T. Haraguchi, and Y. Hiraoka. 1998. Oscillatory nuclear movement in fission yeast meiotic prophase is driven by astral microtubules, as revealed by continuous observation of chromosomes and microtubules in living cells. *J. Cell Sci.* 111:701–712.
- Dissmeyer, N., and A. Schnittger. 2011. The age of protein kinases. *Methods Mol. Biol.* 779:7–52. https://doi.org/10.1007/978-1-61779-264-9_2
- Dissmeyer, N., M.K. Nowack, S. Pusch, H. Stals, D. Inzé, P.E. Grini, and A. Schnittger. 2007. T-loop phosphorylation of *Arabidopsis* CDKA1 is required for its function and can be partially substituted by an aspartate residue. *Plant Cell.* 19:972–985. <https://doi.org/10.1105/tpc.107.050401>
- Dissmeyer, N., A.K. Weimer, S. Pusch, K. De Schutter, C.L. Alvim Kamei, M.K. Nowack, B. Novak, G.-L. Duan, Y.-G. Zhu, L. De Veylder, et al. 2009. Control of cell proliferation, organ growth, and DNA damage response operate independently of dephosphorylation of the *Arabidopsis* Cdk1 homolog CDKA1. *Plant Cell.* 21:3641–3654. <https://doi.org/10.1105/tpc.109.070417>
- Dumitru, A.M.G., S.F. Rusin, A.E.M. Clark, A.N. Kettenbach, and D.A. Compton. 2017. Cyclin A/Cdk1 modulates Plk1 activity in prometaphase to regulate kinetochore-microtubule attachment stability. *eLife.* 6: e29303. <https://doi.org/10.7554/eLife.29303>
- Enami, K., M. Ichikawa, T. Uemura, N. Kutsuna, S. Hasezawa, T. Nakagawa, A. Nakano, and M.H. Sato. 2009. Differential expression control and polarized distribution of plasma membrane-resident SYP1 SNAREs in *Arabidopsis thaliana*. *Plant Cell Physiol.* 50:280–289. <https://doi.org/10.1093/pcp/pcn197>
- Fisher, D.L., and P. Nurse. 1996. A single fission yeast mitotic cyclin B p34cdc2 kinase promotes both S-phase and mitosis in the absence of G1 cyclins. *EMBO J.* 15:850–860. <https://doi.org/10.1002/j.1460-2075.1996.tb00420.x>
- Furness, C.A., and P.J. Rudall. 1999. Microsporogenesis in Monocotyledons. *Ann. Bot.* 84:475–499. <https://doi.org/10.1006/anbo.1999.0942>
- Girard, C., L. Chelysheva, S. Choinard, N. Froger, N. Macaisne, A. Lemhendi, J. Mazel, W. Crismani, and R. Mercier. 2015. AAA-ATPase FIDGETIN-LIKE 1 and Helicase FANCM Antagonize Meiotic Crossovers by Distinct Mechanisms. *PLoS Genet.* 11: e1005369. <https://doi.org/10.1371/journal.pgen.1005369>
- Gutiérrez-Escribano, P., and P. Nurse. 2015. A single cyclin-CDK complex is sufficient for both mitotic and meiotic progression in fission yeast. *Nat. Commun.* 6:6871. <https://doi.org/10.1038/ncomms7871>
- Hajheidari, M., S. Farrona, B. Huettel, Z. Koncz, and C. Koncz. 2012. CDKF1 and CDK protein kinases regulate phosphorylation of serine residues in the C-terminal domain of *Arabidopsis* RNA polymerase II. *Plant Cell.* 24:1626–1642. <https://doi.org/10.1105/tpc.112.096834>
- Harashima, H., and A. Schnittger. 2012. Robust reconstitution of active cell-cycle control complexes from co-expressed proteins in bacteria. *Plant Methods.* 8:23. <https://doi.org/10.1186/1746-4811-8-23>
- Harashima, H., A. Shinmyo, and M. Sekine. 2007. Phosphorylation of threonine 161 in plant cyclin-dependent kinase A is required for cell division by activation of its associated kinase. *Plant J.* 52:435–448. <https://doi.org/10.1111/j.1365-313X.2007.03247.x>
- Henderson, K.A., K. Kee, S. Maleki, P.A. Santini, and S. Keeney. 2006. Cyclin-dependent kinase directly regulates initiation of meiotic recombination. *Cell.* 125(7):1321–1332. <https://doi.org/10.1016/j.cell.2006.04.039>
- Ho, C.-M.K., Y.-R.J. Lee, L.D. Kiyama, S.P. Dinesh-Kumar, and B. Liu. 2012. *Arabidopsis* microtubule-associated protein MAP65-3 cross-links anti-parallel microtubules toward their plus ends in the phragmoplast via its distinct C-terminal microtubule binding domain. *Plant Cell.* 24: 2071–2085. <https://doi.org/10.1105/tpc.111.092569>
- Holt, L.J., B.B. Tuch, J. Villén, A.D. Johnson, S.P. Gygi, and D.O. Morgan. 2009. Global analysis of Cdk1 substrate phosphorylation sites provides insights into evolution. *Science.* 325:1682–1686. <https://doi.org/10.1126/science.1172867>
- Huertas, P., F. Cortés-Ledesma, A.A. Sartori, A. Aguilera, and S.P. Jackson. 2008. CDK targets Sae2 to control DNA-end resection and homologous recombination. *Nature.* 455:689–692. <https://doi.org/10.1038/nature07215>
- Jiang, W., G. Jimenez, N.J. Wells, T.J. Hope, G.M. Wahl, T. Hunter, and R. Fukunaga. 1998. PRC1: a human mitotic spindle-associated CDK substrate protein required for cytokinesis. *Mol. Cell.* 2:877–885. [https://doi.org/10.1016/S1097-2765\(00\)80302-0](https://doi.org/10.1016/S1097-2765(00)80302-0)
- Jürgens, G. 2005. Cytokinesis in higher plants. *Annu. Rev. Plant Biol.* 56: 281–299. <https://doi.org/10.1146/annurev.arplant.55.031903.141636>
- Kaldis, P. 1999. The cdk-activating kinase (CAK): from yeast to mammals. *Cell. Mol. Life Sci.* 55:284–296. <https://doi.org/10.1007/s000180050290>
- Komaki, S., and A. Schnittger. 2017. The Spindle Assembly Checkpoint in *Arabidopsis* Is Rapidly Shut Off during Severe Stress. *Dev. Cell.* 43: 172–185.e5. <https://doi.org/10.1016/j.devcel.2017.09.017>
- Lei, X., and B. Liu. 2020. Tapetum-Dependent Male Meiosis Progression in Plants: Increasing Evidence Emerges. *Front Plant Sci.* 10:1667. <https://doi.org/10.3389/fpls.2019.01667>
- Liu, B., N. De Storme, and D. Geelen. 2017. Gibberellin Induces Diploid Pollen Formation by Interfering with Meiotic Cytokinesis. *Plant Physiol.* 173: 338–353. <https://doi.org/10.1104/pp.16.00480>
- Magnard, J.L., M. Yang, Y.C. Chen, M. Leary, and S. McCormick. 2001. The *Arabidopsis* gene tardy asynchronous meiosis is required for the normal pace and synchrony of cell division during male meiosis. *Plant Physiol.* 127:1157–1166. <https://doi.org/10.1104/pp.010473>
- Mogessie, B., K. Scheffler, and M. Schuh. 2018. Assembly and Positioning of the Oocyte Meiotic Spindle. *Annu. Rev. Cell Dev. Biol.* 34:381–403. <https://doi.org/10.1146/annurev-cellbio-100616-060553>
- Mollinari, C., J.-P. Kleman, W. Jiang, G. Schoehn, T. Hunter, and R.L. Margolis. 2002. PRC1 is a microtubule binding and bundling protein essential to maintain the mitotic spindle midzone. *J. Cell Biol.* 157:1175–1186. <https://doi.org/10.1083/jcb.200111052>
- Morgan, D.O. 1997. Cyclin-dependent kinases: engines, clocks, and micro-processors. *Annu. Rev. Cell Dev. Biol.* 13:261–291. <https://doi.org/10.1146/annurev.cellbio.13.1.261>
- Müller, S., and G. Jürgens. 2016. Plant cytokinesis-No ring, no constriction but centrifugal construction of the partitioning membrane. *Semin. Cell Dev. Biol.* 53:10–18. <https://doi.org/10.1016/j.semcdb.2015.10.037>

- Nakagawa, T., T. Suzuki, S. Murata, S. Nakamura, T. Hino, K. Maeo, R. Tabata, T. Kawai, K. Tanaka, Y. Niwa, et al. 2007. Improved Gateway binary vectors: high-performance vectors for creation of fusion constructs in transgenic analysis of plants. *Biosci. Biotechnol. Biochem.* 71: 2095–2100. <https://doi.org/10.1271/bbb.70216>
- Nannas, N.J., D.M. Higgins, and R.K. Dawe. 2016. Anaphase asymmetry and dynamic repositioning of the division plane during maize meiosis. *J. Cell Sci.* 129:4014–4024. <https://doi.org/10.1242/jcs.194860>
- Nowack, M.K., P.E. Grini, M.J. Jakoby, M. Lafos, C. Koncz, and A. Schnittger. 2006. A positive signal from the fertilization of the egg cell sets off endosperm proliferation in angiosperm embryogenesis. *Nat. Genet.* 38: 63–67. <https://doi.org/10.1038/ng1694>
- Nowack, M.K., H. Harashima, N. Dissmeyer, X. Zhao, D. Bouyer, A.K. Weimer, F. De Winter, F. Yang, and A. Schnittger. 2012. Genetic framework of cyclin-dependent kinase function in Arabidopsis. *Dev. Cell.* 22:1030–1040. <https://doi.org/10.1016/j.devcel.2012.02.015>
- Ortega, S., I. Prieto, J. Odajima, A. Martin, P. Dubus, R. Sotillo, J.L. Barbero, M. Malumbres, and M. Barbacid. 2003. Cyclin-dependent kinase 2 is essential for meiosis but not for mitotic cell division in mice. *Nat. Genet.* 35:25–31. <https://doi.org/10.1038/ng1232>
- Pagliuca, F.W., M.O. Collins, A. Lichawski, P. Zegerman, J.S. Choudhary, and J. Pines. 2011. Quantitative proteomics reveals the basis for the biochemical specificity of the cell-cycle machinery. *Mol. Cell.* 43:406–417. <https://doi.org/10.1016/j.molcel.2011.05.031>
- Park, M., C. Krause, M. Karnahl, I. Reichardt, F. El Kasmi, U. Mayer, Y.-D. Stierhof, U. Hiller, G. Strompen, M. Bayer, et al. 2018. Concerted Action of Evolutionarily Ancient and Novel SNARE Complexes in Flowering-Plant Cytokinesis. *Dev. Cell.* 44:500–511.e4. <https://doi.org/10.1016/j.devcel.2017.12.027>
- Pesin, J.A., and T.L. Orr-Weaver. 2008. Regulation of APC/C activators in mitosis and meiosis. *Annu. Rev. Cell Dev. Biol.* 24:475–499. <https://doi.org/10.1146/annurev.cellbio.041408.115949>
- Peterson, R., J.P. Slovin, and C. Chen. 2010. A simplified method for differential staining of aborted and non-aborted pollen grains. *Int. J. Plant Biol.* 1. e13. <https://doi.org/10.4081/pb.2010.e13>
- Prusicki, M.A., E.M. Keizer, R.P. van Rosmalen, S. Komaki, F. Seifert, K. Müller, E. Wijnker, C. Fleck, and A. Schnittger. 2019. Live cell imaging of meiosis in Arabidopsis thaliana. *eLife.* 8. e42834. <https://doi.org/10.7554/eLife.42834>
- Pusch, S., H. Harashima, and A. Schnittger. 2012. Identification of kinase substrates by bimolecular complementation assays. *Plant J.* 70:348–356. <https://doi.org/10.1111/j.1365-313X.2011.04862.x>
- Ressayre, A., L. Dreyer, S. Triki-Teurtroy, A. Forchioni, and S. Nadot. 2005. Post-meiotic cytokinesis and pollen aperture pattern ontogeny: comparison of development in four species differing in aperture pattern. *Am. J. Bot.* 92:576–583. <https://doi.org/10.3732/ajb.92.4.576>
- Ross, K.J., P. Fransz, and G.H. Jones. 1996. A light microscopic atlas of meiosis in Arabidopsis thaliana. *Chromosome Res.* 4:507–516. <https://doi.org/10.1007/BF02261778>
- Santamaría, D., C. Barrière, A. Cerqueira, S. Hunt, C. Tardy, K. Newton, J.F. Cáceres, P. Dubus, M. Malumbres, and M. Barbacid. 2007. Cdk1 is sufficient to drive the mammalian cell cycle. *Nature.* 448:811–815. <https://doi.org/10.1038/nature06046>
- Sasabe, M., V. Boudolf, L. De Veylder, D. Inzé, P. Genschik, and Y. Machida. 2011. Phosphorylation of a mitotic kinesin-like protein and a MAPKKK by cyclin-dependent kinases (CDKs) is involved in the transition to cytokinesis in plants. *Proc. Natl. Acad. Sci. USA.* 108:17844–17849. <https://doi.org/10.1073/pnas.1110174108>
- Satyanarayana, A., C. Berthet, J. Lopez-Molina, V. Coppola, L. Tessarollo, and P. Kaldis. 2008. Genetic substitution of Cdk1 by Cdk2 leads to embryonic lethality and loss of meiotic function of Cdk2. *Development.* 135(20): 3389–3400. <https://doi.org/10.1242/dev.024919>
- Shamina, N.V., E.I. Gordeeva, N.M. Kovaleva, E.G. Seriyukova, and N.V. Dorogova. 2007. Formation and function of phragmoplast during successive cytokinesis stages in higher plant meiosis. *Cell Biol. Int.* 31: 626–635. <https://doi.org/10.1016/j.cellbi.2006.12.001>
- Shimotohno, A., S. Matsubayashi, M. Yamaguchi, H. Uchimiya, and M. Umeda. 2003. Differential phosphorylation activities of CDK-activating kinases in Arabidopsis thaliana. *FEBS Lett.* 534:69–74. [https://doi.org/10.1016/S0014-5793\(02\)03780-8](https://doi.org/10.1016/S0014-5793(02)03780-8)
- Shimotohno, A., R. Ohno, K. Bisova, N. Sakaguchi, J. Huang, C. Koncz, H. Uchimiya, and M. Umeda. 2006. Diverse phosphoregulatory mechanisms controlling cyclin-dependent kinase-activating kinases in Arabidopsis. *Plant J.* 47:701–710. <https://doi.org/10.1111/j.1365-313X.2006.02820.x>
- Smertenko, A., F. Assaad, F. Baluška, M. Bezanilla, H. Buschmann, G. Drakakaki, M.-T. Hauser, M. Janson, Y. Mineyuki, I. Moore, et al. 2017. Plant Cytokinesis: Terminology for Structures and Processes. *Trends Cell Biol.* 27:885–894. <https://doi.org/10.1016/j.tcb.2017.08.008>
- Stern, B., and P. Nurse. 1996. A quantitative model for the cdc2 control of S phase and mitosis in fission yeast. *Trends Genet.* 12:345–350. [https://doi.org/10.1016/S0168-9525\(96\)80016-3](https://doi.org/10.1016/S0168-9525(96)80016-3)
- Takatsuka, H., C. Umeda-Hara, and M. Umeda. 2015. Cyclin-dependent kinase-activating kinases CDK1 and CDK3 are essential for preserving mitotic activity in Arabidopsis thaliana. *Plant J.* 82:1004–1017. <https://doi.org/10.1111/tj.12872>
- Tapley, E.C., and D.A. Starr. 2013. Connecting the nucleus to the cytoskeleton by SUN-KASH bridges across the nuclear envelope. *Curr. Opin. Cell Biol.* 25:57–62. <https://doi.org/10.1016/j.ceb.2012.10.014>
- Tyson, J.J., and B. Novák. 2015. Models in biology: lessons from modeling regulation of the eukaryotic cell cycle. *BMC Biol.* 13:46. <https://doi.org/10.1186/s12915-015-0158-9>
- Ubersax, J.A., E.L. Woodbury, P.N. Quang, M. Paraz, J.D. Blethrow, K. Shah, K.M. Shokat, and D.O. Morgan. 2003. Targets of the cyclin-dependent kinase Cdk1. *Nature.* 425:859–864. <https://doi.org/10.1038/nature02062>
- Umeda, M., A. Shimotohno, and M. Yamaguchi. 2005. Control of cell division and transcription by cyclin-dependent kinase-activating kinases in plants. *Plant Cell Physiol.* 46:1437–1442. <https://doi.org/10.1093/pcp/pci170>
- Van Leene, J., J. Hollunder, D. Eeckhout, G. Persiau, E. Van De Slijke, H. Stals, Van Isterdael, A. Verkest, S. Neiryneck, Y. Buffel, et al. 2010. Targeted interactomics reveals a complex core cell cycle machinery in Arabidopsis thaliana. *Mol. Syst. Biol.* 6:397. <https://doi.org/10.1038/msb.2010.53>
- Vavrdová, T., J. Samaj, and G. Komis. 2019. Phosphorylation of Plant Microtubule-Associated Proteins During Cell Division. *Front Plant Sci.* 10:238. <https://doi.org/10.3389/fpls.2019.00238>
- Wang, G., H. Kong, Y. Sun, X. Zhang, W. Zhang, N. Altman, C.W. DePamphilis, and H. Ma. 2004a. Genome-wide analysis of the cyclin family in Arabidopsis and comparative phylogenetic analysis of plant cyclin-like proteins. *Plant Physiol.* 135:1084–1099. <https://doi.org/10.1104/pp.104.040436>
- Wang, Y., J.-L. Magnard, S. McCormick, and M. Yang. 2004b. Progression through meiosis I and meiosis II in Arabidopsis anthers is regulated by an A-type cyclin predominately expressed in prophase I. *Plant Physiol.* 136:4127–4135. <https://doi.org/10.1104/pp.104.051201>
- Weimer, A.K., M.K. Nowack, D. Bouyer, X. Zhao, H. Harashima, S. Naseer, F. De Winter, N. Dissmeyer, N. Geldner, and A. Schnittger. 2012. Retinoblastoma related1 regulates asymmetric cell divisions in Arabidopsis. *Plant Cell.* 24:4083–4095. <https://doi.org/10.1105/tpc.112.10.4620>
- Weingartner, M., P. Binarova, D. Drykova, A. Schweighofer, J.-P. David, E. Heberle-Bors, J. Doonan, and L. Bögre. 2001. Dynamic recruitment of Cdc2 to specific microtubule structures during mitosis. *Plant Cell.* 13: 1929–1943. <https://doi.org/10.1105/TPC.010109>
- Weingartner, M., M.-C. Criqui, T. Mészáros, P. Binarova, A.-C. Schmit, A. Helfer, A. Drevier, M. Erhardt, L. Bögre, and P. Genschik. 2004. Expression of a nondegradable cyclin B1 affects plant development and leads to endomitosis by inhibiting the formation of a phragmoplast. *Plant Cell.* 16:643–657. <https://doi.org/10.1105/tpc.020057>
- Wijnker, E., H. Harashima, K. Müller, P. Parra-Núñez, C.B. de Snoo, J. van de Belt, N. Dissmeyer, M. Bayer, M. Pradillo, and A. Schnittger. 2019. The Cdk1/Cdk2 homolog CDKA;1 controls the recombination landscape in Arabidopsis. *Proc. Natl. Acad. Sci. USA.* 116:12534–12539. <https://doi.org/10.1073/pnas.1820753116>
- Yang, C., Y. Hamamura, K. Sofroni, F. Böwer, S.C. Stolze, H. Nakagami, and A. Schnittger. 2019. SWITCH 1/DYAD is a WINGS APART-LIKE antagonist that maintains sister chromatid cohesion in meiosis. *Nat. Commun.* 10: 1755. <https://doi.org/10.1038/s41467-019-09759-w>
- Yang, C., K. Sofroni, E. Wijnker, Y. Hamamura, L. Carstens, H. Harashima, S.C. Stolze, D. Vezon, L. Chelysheva, Z. Orban-Nemeth, et al. 2020. The Arabidopsis Cdk1/Cdk2 homolog CDKA;1 controls chromosome axis assembly during plant meiosis. *EMBO J.* 39. e101625. <https://doi.org/10.15252/embj.2019101625>
- Yoshida, M., S. Katsuyama, K. Tateho, H. Nakamura, J. Miyoshi, T. Ohba, H. Matsuura, F. Miki, K. Okazaki, T. Haraguchi, et al. 2013. Microtubule-organizing center formation at telomeres induces meiotic telomere clustering. *J. Cell Biol.* 200:385–395. <https://doi.org/10.1083/jcb.201207168>
- Zhao, X., H. Harashima, N. Dissmeyer, S. Pusch, A.K. Weimer, J. Bramsiepe, D. Bouyer, S. Rademacher, M.K. Nowack, B. Novak, et al. 2012. A general G1/S-phase cell-cycle control module in the flowering plant Arabidopsis thaliana. *PLoS Genet.* 8. e1002847. <https://doi.org/10.1371/journal.pgen.1002847>

Supplemental material

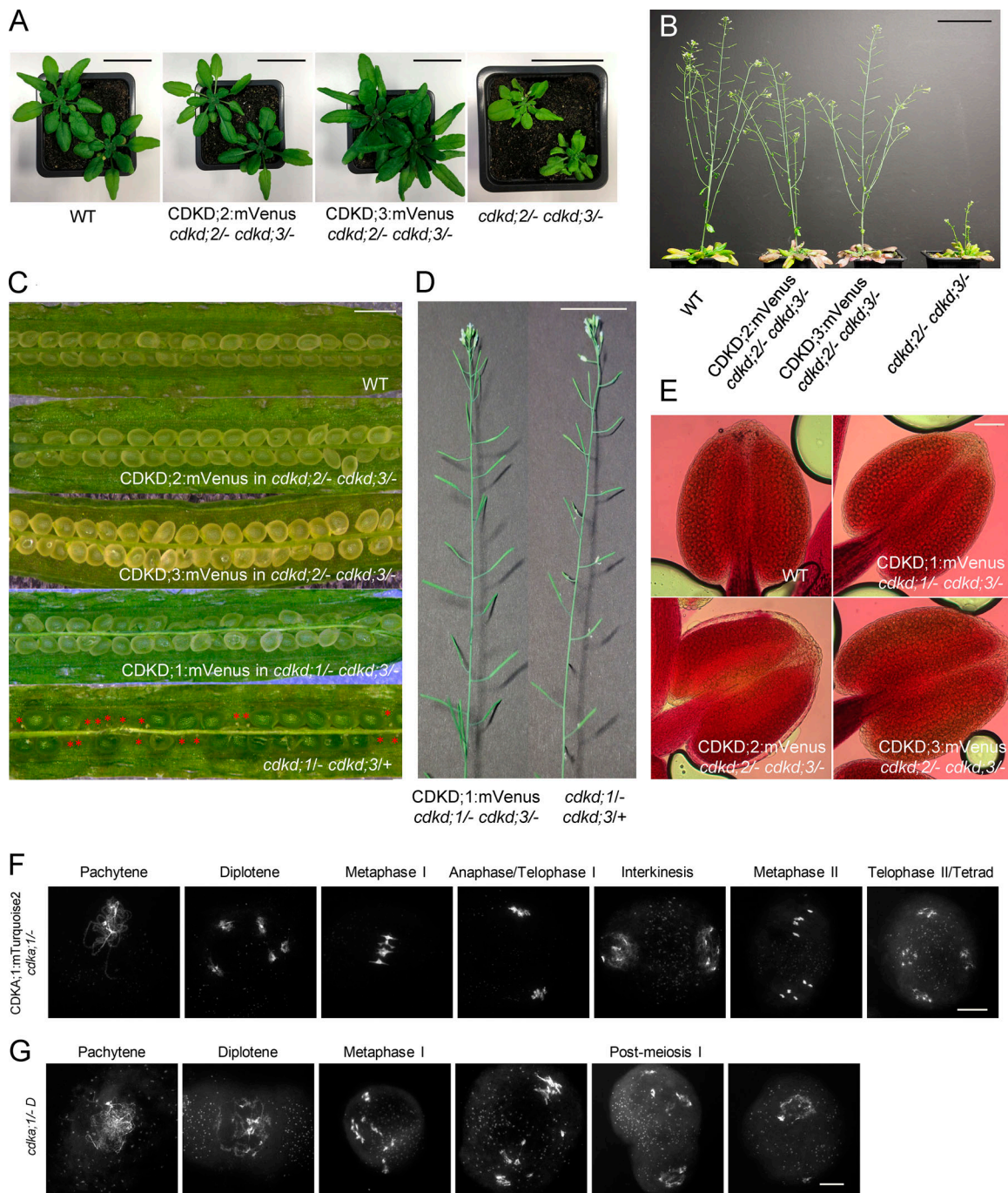


Figure S1. **The *CDKD;1*, *CDKD;2*, *CDKD;3*, and *CDKA;1* reporter constructs are fully functional.** (A) Phenotypes of *cdkd;2*^{-/-} *cdkd;3*^{-/-} double mutants and *cdkd;2*^{-/-} *cdkd;3*^{-/-} double mutants containing a *CDKD;2* and *CDKD;3* reporter, respectively, in comparison with WT. Photographs were taken 5 wk after sowing. Scale bar, 3 cm. (B) Inflorescences of the *cdkd;2*^{-/-} *cdkd;3*^{-/-} double mutants and the *CDKD;2* and *CDKD;3* reporter lines (in a *cdkd;2*^{-/-} *cdkd;3*^{-/-} mutant background) in comparison with WT plants of the same age. Photographs were taken 14 wk after sowing. Scale bar, 7 cm. (C) Siliques of WT, the *CDKD;2* and *CDKD;3* reporters in a *cdkd;2*^{-/-} *cdkd;3*^{-/-} mutant background, and the *CDKD;1* reporter in a *cdkd;1*^{-/-} *cdkd;3*^{-/-} mutant background versus *cdkd;1*^{-/-} *cdkd;3*^{+/+} double mutants, which have a high level of seed abortion, indicated by red asterisks. Scale bar, 1 mm. (D) The main stem and siliques of the *CDKD;1* reporter line in a *cdkd;1*^{-/-} *cdkd;3*^{-/-} background versus *cdkd;1*^{-/-} *cdkd;3*^{+/+} double mutant. Scale bar, 3 cm. (E) Peterson staining of anthers for WT, *CDKD;1*, *CDKD;2* and *CDKD;3* reporter lines in the indicated *cdkd* mutant background. Scale bar, 20 μm. (F and G) Chromosome spread analysis of *CDKA;1:mTurquoise2* in *cdkd;1*^{-/-} (F) versus *cdka;1*^{-/-} *D* mutant (G). Scale bar, 10 μm.

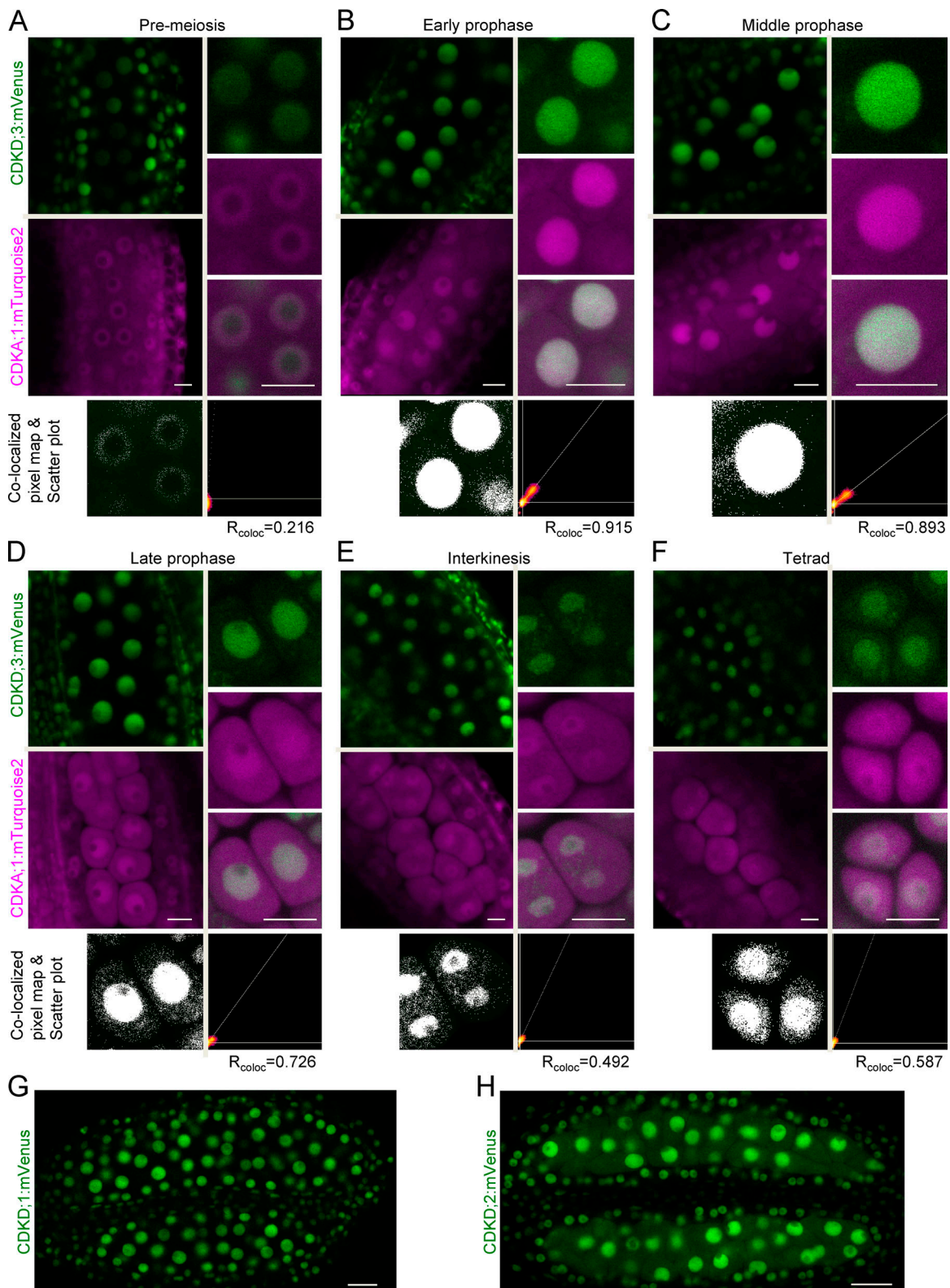


Figure S2. **CDKD;3 and CDKA;1 are expressed throughout meiosis and colocalize in the nucleus.** Confocal laser scanning micrographs showing the localization of the functional CDKD;3:mVenus (green) and CDKA;1:mTurquoise2 (magenta) fusion proteins in male anthers of *Arabidopsis*. **(A–F)** During prophase I (A–D), interkinesis (E), and tetrad stage (F), both proteins enrich and differentially colocalize in the meiocyte nucleus, as shown in every third row by the colocalized pixel map and scatter plot. The diagonal white line in the scatter plot represents the ratio of the intensities of the two channels (R_{coloc}). Scale bar, 10 μ m. **(G)** Confocal laser scanning micrographs of anthers showing the accumulation of the CDKD;1:mVenus fusion protein in green. **(H)** Accumulation pattern of the CDKD;2:mVenus fusion protein in whole anthers. Scale bar, 20 μ m.

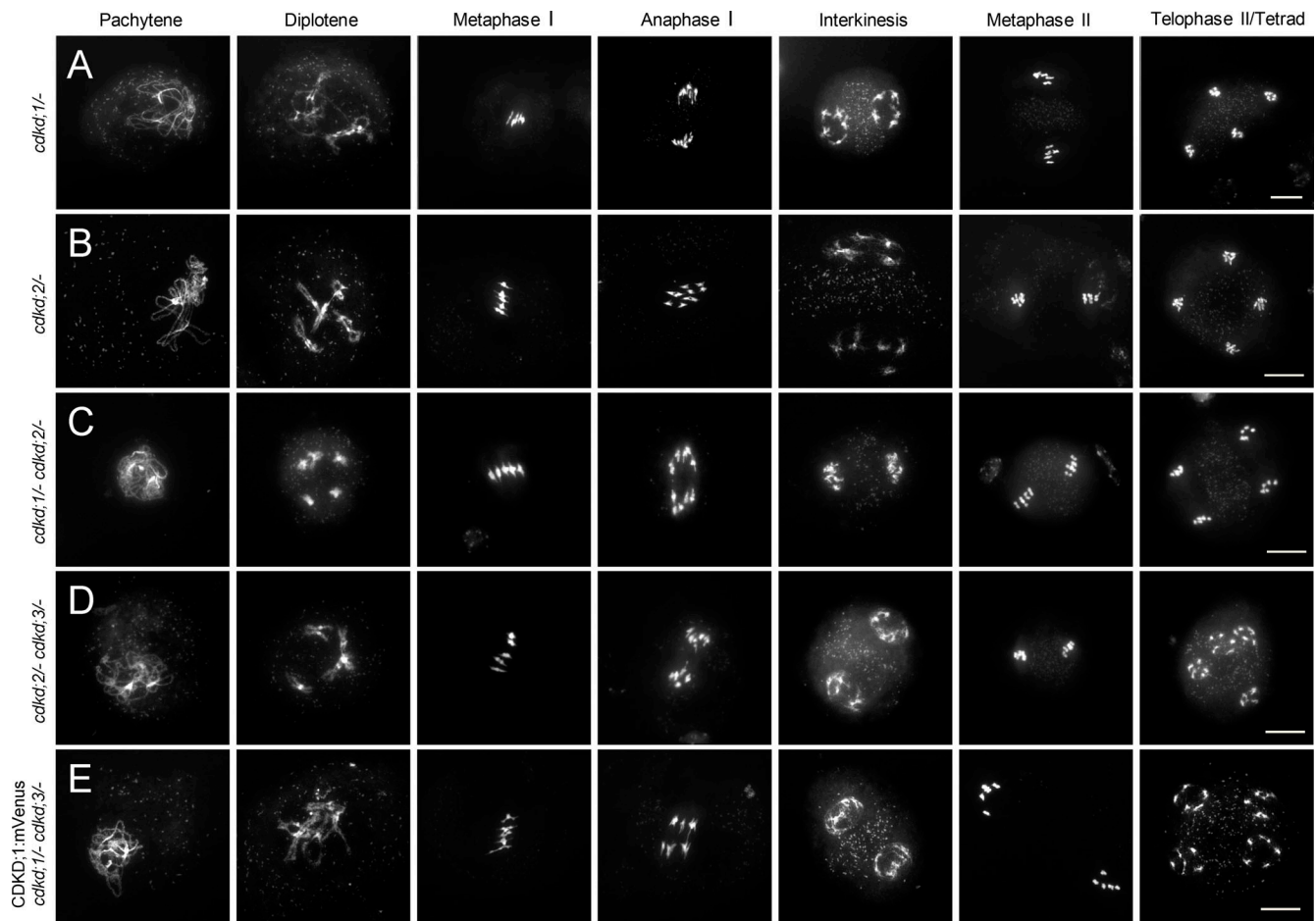


Figure S3. **Chromosome spreads of single and double *cdkd* mutants and CDKD reporter lines used in this study.** (A–E) Chromosome spreads with WT-like meiotic progression in *cdkd;1*– (A), *cdkd;2*– (B), *cdkd;1*– *cdkd;2*– (C), *cdkd;2*– *cdkd;3*– (D), and *CDKD;1:mVenus* in *cdkd;1*– *cdkd;3*– (E). Scale bar, 10 μ m.

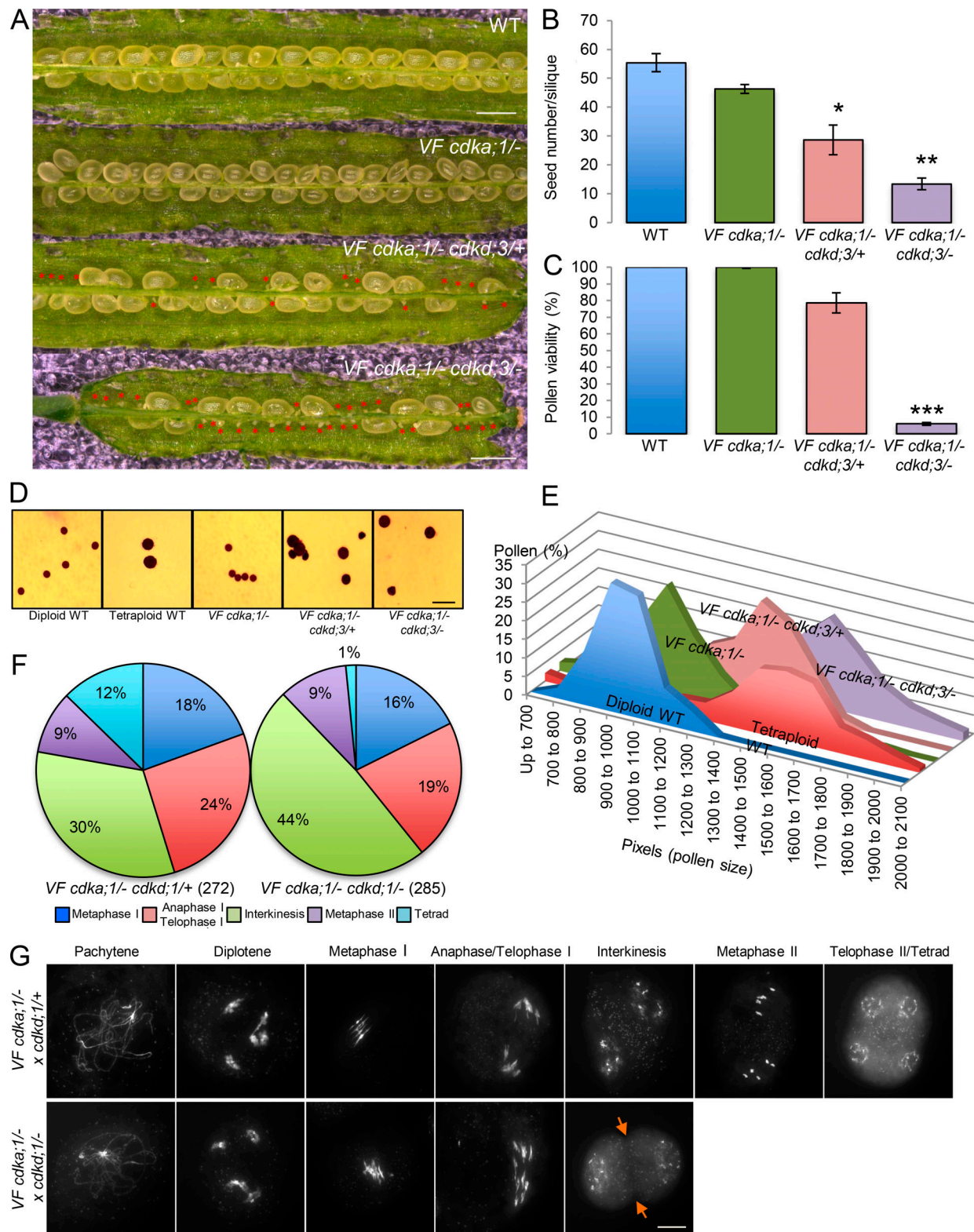
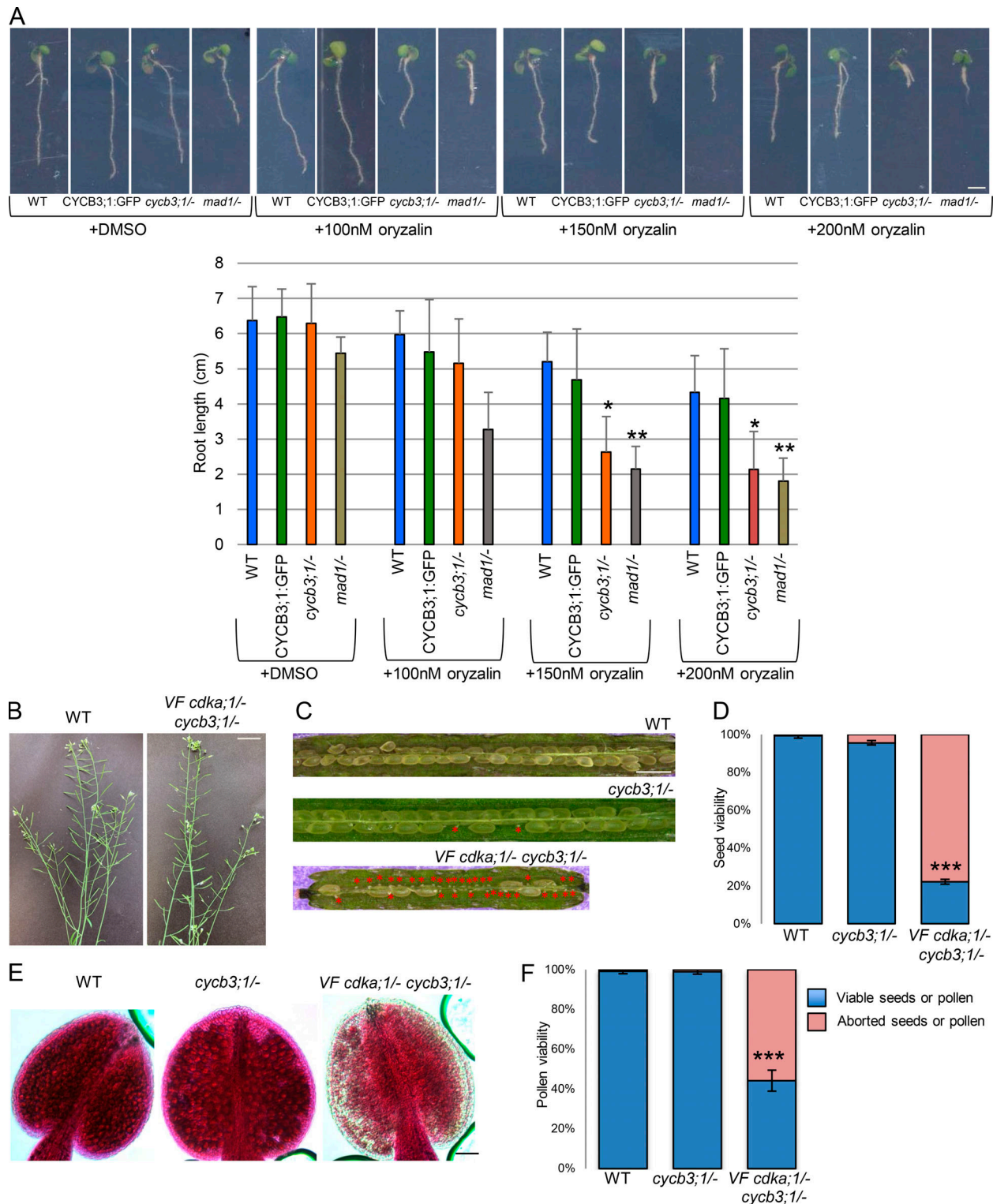


Figure S4. **Phenotypic characterization of *VF cdk1;1 cdk1;3* and *VF cdk1;1 cdk1;1* mutant combinations.** (A) Siliques of WT versus *VF cdk1;1/-*, *VF cdk1;1/- cdk1;3/+*, and *VF cdk1;1/- cdk1;3/-*. Red asterisks indicate aborted seeds. Scale bar, 1 mm. (B and C) Number of aborted seeds in at least five siliques (B) and pollen viability using at least eight flower buds (C) for the genotypes shown in A. Level of significance (*, $P < 0.05$; **, $P < 0.01$; ****, $P < 0.001$) determined by one-way ANOVA followed by Tukey's test. (D) Pollen sizes (in pixels) after Peterson staining of diploid and tetraploid WT pollen versus pollen from *VF cdk1;1/-*, *VF cdk1;1/- cdk1;3/+*, and *VF cdk1;1/- cdk1;3/-* from ≥ 500 pollen grains for each genotype. (E) Peterson staining revealing the difference in pollen size for the genotypes quantified in D. Scale bar, 20 μm . (F) Repartition of meiotic stages within one flower bud undergoing meiosis from metaphase I to telophase II/tetrad in *VF cdk1;1/- cdk1;1/+* ($n = 272$) and *VF cdk1;1/- cdk1;1/-* ($n = 285$). (G) Chromosome spread analysis of male meiocytes of *VF cdk1;1/- cdk1;1/+* and *VF cdk1;1/- cdk1;1/-*. Orange arrows highlight the premature exit after meiosis I in 75% of the meiocytes analyzed. Scale bar, 10 μm .



Video 1. **Meiotic progression from late prophase to tetrad formation. (A and B)** Meiotic progression from late prophase to tetrad formation in two anthers of a WT flower (A) and in one anther of a *VF cdk;1/-* mutant plant (B). Tubulin (RFP) in magenta highlights microtubules during meiosis I to meiosis II transition. The interval between image acquisitions is 7 min. Time format (h:min). Scale bar, 10 μ m. Frame rate is 5 frames per second.

Video 2. **Successive cytokinesis in one anther of a *VF cdk;1/- cdk;3/+* mutant flower.** Tubulin (RFP) in magenta highlights microtubules from late prophase to tetrad formation, and the bright-field image (cell shape) appears in gray. Cell wall deposition is observed after the first meiotic division (first cytokinesis), followed by the assembly of two spindles and a second cell wall deposition after the second meiotic division (second cytokinesis). See also Fig. 5 B. The interval between image acquisitions is 10 min. Time format (h:min). Scale bar, 10 μ m. Frame rate is 5 frames per second.

Video 3. **Meiotic exit after the first division in one anther of a *VF cdk;1/- cdk;3/-* mutant flower.** Tubulin (RFP) in magenta highlights microtubules from late prophase to dyad formation, and the bright-field image (cell shape) appears in gray. Cell wall deposition is observed after the first meiotic division, and meiocytes do not progress through a second division. See also Fig. 5 C. The interval between image acquisitions is 10 min. Time format (h:min). Scale bar, 10 μ m. Frame rate is 5 frames per second.

Video 4. **Plasma membrane dynamics during simultaneous cytokinesis in WT and meiotic exit in *VF cdk;1/- cdk;3/-*.** SYP132 (GFP) in green highlights the plasma membrane during the simultaneous cell wall deposition in WT (white box, left panel) leading to the formation of a tetrad. In contrast, premature cell wall deposition in *VF cdk;1/- cdk;3/-* (white box, right panel) causes the formation of a dyad. In both cases, cell wall deposition follows the same direction, i.e., from the outside to the inside. See also Fig. 5 D. Time format (h:min). Scale bar, 10 μ m. Frame rate is 5 frames per second.

Video 5. **MAP65-3 is loaded twice at interkinesis and tetrad formation during WT meiosis.** Progression of meiosis from late prophase to tetrad in one anther of WT flowers. MAP65-3 (GFP) is highlighted in green, and tubulin (RFP) in magenta. Note the appearance of MAP65-3 at the onset of anaphase I and II and its localization at the midzone in interkinesis and telophase II. See also Fig. 6 D. The interval between image acquisitions is 5 min. Scale bar, 10 μ m. Frame rate is 5 frames per second.

Video 6. **Dynamics of MAP65-3 in plants with low CDK levels.** Comparison of meiotic progression in one anther of WT (left) and *VF cdk;1/- cdk;3/-* mutant (right). MAP65-3 (GFP) in green highlights premature antiparallel microtubule bundle structures before NEB. Moreover, the pattern of MAP65-3 localization is more diffuse and less regular in comparison with WT. See also Fig. 6 I. The interval between image acquisitions is 10 min. Scale bar, 10 μ m. Frame rate is 5 frames per second.

Video 7. **CYCB3;1 localizes to the first meiotic spindle.** Progression of meiosis from late prophase to tetrad formation in one anther of WT flowers. CYCB3;1 (GFP) is highlighted in green (first panel), tubulin (RFP) in magenta (second panel), and their merge in the last panel. CYCB3;1 is strongly associated with the first but not the second spindle. See also Fig. 8 B. The interval between image acquisitions is 5 min. Scale bar, 10 μ m. Frame rate is 5 frames per second.

Video 8. **Meiotic progression from mid-prophase (half-moon stage) to tetrad formation in one anther of WT treated with DMSO (left) versus *cyb3;1* treated with DMSO (right).** Tubulin (RFP) is highlighted in white. Note that microtubules are not affected, and the meiocytes progress through meiosis as untreated flowers. See also Fig. 9, B and C. The interval between image acquisitions is 10 min. Scale bar, 10 μ m. Frame rate is 8 frames per second.

Video 9. **Meiotic progression from middle prophase (half-moon stage) to tetrad formation in two anthers of WT treated with 200 nM oryzalin (left) versus *cyb3;1/-* treated with 200 nM oryzalin (right).** Tubulin (RFP) is highlighted in white. While microtubules are not affected in WT, the spindle length is reduced in treated *cyb3;1/-*. See also Fig. 9, D and E. The interval between image acquisitions is 10 min. Scale bar, 10 μ m. Frame rate is 12 frames per second.

Video 10. **Meiotic progression from middle prophase (half-moon stage) in two anthers of WT treated with 500 nM oryzalin (left) versus *cycb3;1*^{-/-} treated with 500 nM oryzalin (right).** Tubulin (RFP) is highlighted in white. In treated WT flowers, meiotic spindles are shorter in comparison with untreated flowers or flowers treated with lower concentrations of oryzalin (left panel). In contrast, spindles are completely absent in treated *cycb3;1*^{-/-} mutants (right panel). In addition, microtubules are very diffuse in *cycb3;1*^{-/-} mutants (right panel), and after two NEB events, the formation of completely unreduced gametes is observed. See also [Fig. 9, F and G](#). The interval between image acquisitions is 10 min. Scale bar, 10 μ m. Frame rate is 12 frames per second.

Provided online is one table. Table S1 lists the primers used in this study.